Optimal Sizing and Operation of Energy Storage Systems to Mitigate Intermittency of Renewable Energy Resources

by

Iman Naziri Moghaddam

A thesis submitted to the faculty of
The University of North Carolina at Charlotte
In partial fulfillment of the requirements
For the degree of PhD in Electrical Engineering

Charlotte

2018

Approved by:

Dr. Chowdhury

Dr. Salami

Prof. Kakad

Dr. Lim

ABSTRACT

IMAN NAZIRI MOGHADDAM. Optimal Sizing and Operation of Energy Storage Systems to Mitigate Intermittency of Renewable Energy Resources. (Under the direction of PROF. BADRUL CHOWDHURY)

Increased share of Renewable Energy Sources (RES) in the generation mix requires higher flexibility in power system resources. The intermittent nature of the RES calls for higher reserves in power systems to smooth out the unpredictable power fluctuations. Grid-tied energy storage systems are practical solutions to facilitate the massive integration of RES. The deployment of Battery Energy Storage Systems (BESS) on the power grids is experiencing a significant growth in recent years. Thanks to intensive research and development in battery chemistry and power conversion systems, BESS costs are reducing. However, much more advancements in battery manufacturing as well as additional incentives from the market side are still needed to make BESS a more cost-effective solution. Planning and operation of the BESS significantly influence its profitability. It is quite important to find optimal sizes of batteries and inverters. Sizing of the BESS for two different applications is addressed in this work. In the first application, the BESS is co-located with Pumped Storage Hydro (PSH) to meet the Day-Ahead (DA) schedule of wind generation. In the second application, a method for BESS sizing in the presence of PV-induced ramp rate limits is proposed. In this thesis, two methods based on Receding Horizon Control (RHC) for the optimal operation of the BESS are introduced. A co-located BESS and wind farm is considered in both methods. In one method, electricity market participation is not considered, and the goal is solely meeting the DA schedule utilizing the

BESS. A novel predictive control method is proposed in this part and the efficiency of the method is evaluated through long-run simulations using actual historical wind power.

In the second scenario, market participation of the BESS is taken into account. The deviation from the DA schedule can be compensated through the BESS, or by purchasing power from the real-time electricity market. The optimization problem based on physical and operational constraints is developed. The problem is solved through an RHC scheme while using updated wind power and electricity price forecasts. In this thesis, a Ridge-regression forecast model for electricity price and an ARIMA forecast model for wind power are developed. Simulation results using actual historical data for wind power and electricity price demonstrate that the proposed algorithm increases the average daily profit. In order to evaluate the impact of the BESS lifetime and price on average daily profit, different scenarios are defined and simulated. Although they increase the complexity of the problem, much more realistic result might be obtained when all details and constraints are considered.

To my parents, Masoud and Nafiseh.
And to my sisters, Elham and Elnaz.
And my beloved wife, Lina.
without whom I would not be here today.

ACKNOWLEDGMENTS

I am extremely excited that I have finally completed this complicated winding path toward my PhD. This journey was not easy nor short, and would not have been completed without the help of some gracious people. I wish to express my sincere thanks to my advisor, Prof. Badrul Chowdhury, for his valuable guidance, encouragement, and constant support throughout my PhD. He is an example of a perfect mentor, a remarkable researcher, and an incredible instructor. Besides my advisor, I was fortunate to have Dr. Zia Salami, Dr. Yogendra Kakad, and Dr. Churlzu Lim on my PhD committee. I am grateful for their insightful comments. I would like to thank Dr. Zia Salami for his unconditional support and guidance at the beginning of my path and I will remain indebted to him.

I also would like to thank my colleagues and friends. First, I want to thank Saeed Mohajeryami and Milad Doostan for providing valuable inputs on different stages of this work. Moreover, I take this opportunity to record my sincere thanks to all of my friends in ECE for sharing their knowledge and giving insightful comments. To name a few, I would like to acknowledge Reza Yousefian, Behdad Vatani, Masoud Davoudi, and Mehrdad Biglarbeigian.

Also, I want to thank my wonderful wife, Lina, for her tremendous encouragement, support, and sacrifice. She has always been beside me all these years and made my life more enjoyable with her love and support. Finally, I wish to thank my parents, Nafiseh Masoudnia and Masoud Naziri Moghaddam, who have raised me with love and I would not have been here without their support. Their unconditional love, encouragement, and guidance have motivated me to pursue my goals.

LIST OF CONTENTS

LIST OF FIGURES

CHAPTER 1: MOTIVATION AND PROBLEM OVERVIEW

1.1 Motivation

Wind power, as a valuable renewable energy resource, is experiencing an unprecedented surge in recent years. The US government has set a national mandatory Renewable Energy Target (RET) of 20% by 2020 [1] . Nevertheless, many states have set higher renewables penetration as their individual targets. Similarly, the European Renewable Energy Council (EREC) has released its roadmap for increasing renewable energy penetration to 20% by 2020 [2] . Presently, the contribution of renewable resources shows photovoltaics having the highest rate of growth and wind power having the larger share of generation.

Large wind farms are mainly connected to transmission networks due to robustness of the high voltage transmission interconnected system. Although there are some concerns about the impact of wind variability on voltage imbalance on the distribution network, small wind turbines may connect at the distribution level. However, low X/R ratio and the radial structure of distribution networks prevent high penetration of distributed generation [3]. Variations in power generation cause voltage variations on distribution networks, and to some extent, on transmission systems. This voltage variation may lead to voltage instability, power loss increase, etc. Thus, as renewable energy penetration increases, the role of energy storage systems cannot be underestimated. Keeping the power output of wind farms within the scheduled limit may be done by adding energy storage to the system.

The primary obstacle to deployment of BESS in power networks is the high cost of batteries. For instance, Li-ion and Sodium-Sulfur (NaS) batteries cost 300-500 $/kWh,

depending on the power rating. In addition, lead-acid types costs 150-250 $/kWh and Zinc-Bromine batteries cost 200-400 $/kWh [4]- [5]. Li-ion and NaS batteries are capturing a larger portion of the market due to their fast response and life cycle model. Lead-acid batteries still encounter the sudden failure problem, which eliminate them from safe and reliable options. The following figure shows the trend of the battery price for Electric Vehicles (EV) [6] The trend is similar for batteries meant for stationary applications.

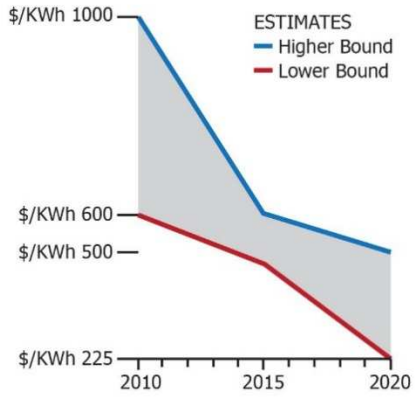

Figure 1-1 Estimation and trend of battery price

Finding an optimal power and energy capacity for a battery energy storage is a crucial concern. Various types of batteries are suitable for different applications. Some types can support high power rating, while others are suitable for high-energy rating. Fast acting batteries with high power capacity are a good fit for frequency regulation services (regulation up/down and responsive reserves). Conversely, high-energy capacity batteries may be utilized for energy arbitrage and balancing services. This main objective of this work is to find the optimal size of energy storage and optimal operation to facilitate high penetration of renewable energy resources in power networks.

1.2 Methods for Sizing of Energy Storage

One of the major concerns in high penetration of renewable energy resources is the impact on frequency deviations on the grid [7]- [8]. The governor and rotor inertia of synchronous generators in conventional power plants can compensate for minor frequency deviations [9]. However, the increasing level of renewable energy resources calls for additional reserves and better coordination in the network. Energy Storage Systems (ESS) is such a solution to mitigate the adverse effects of the variability that accompanies renewable energy resources.

In this chapter, different methods for sizing of energy storage for renewable energy integration are addressed. First, a simple method of battery and inverter sizing is reviewed for solar application based on simulation of historical data. Then, a generic method for sizing of BESS for smoothing out the power generation of large PV farms is introduced. Then it will be shown how control (charge/discharge) strategy of the BESS affects the required battery size to mitigate the solar farm's output. Better performance of a BESS results in smaller size of battery and inverter.

In the next part of this chapter, two or more energy storage systems coordinated together, as a more cost-effective solution, are considered to mitigate the intermittency of wind energy. A novel frequency-based method is used to optimally size two or more different types of energy storage systems.

Different ESS technologies have varying performances over a time horizon. Some technologies such as Pumped Storage Hydro (PSH) and Compressed Air Energy Storage (CAES) are useful in slow cycles due to their ramp rates. On the contrary, a number of

technologies, like BESS and supercapacitors, are cost-efficient in small and frequent variations.

The time horizon of imbalance power can be decomposed into intra-day, intra-hour, and real-time components using frequency domain components. Hence, ESSs can be employed based on their efficiency in the different time spans. The Discrete Fourier transform (DFT) is one of the methods to decompose time horizon data into high frequency and low frequency components.

Mainly, energy storage sizing is about finding minimum power and energy capacity of ESS to mitigate wind power forecast error. Needless to say, a larger ESS results in smaller power forecast errors and higher ESS costs. Thus, there is a tradeoff between the ESS size and its capital cost. Most of the research work seen in the literature have addressed optimal ESS sizing for only one ESS technology. However, different ESS technologies can operate together to improve their performance. Hybrid Energy Storage Systems (HESS) refers to two or more ESS technologies with their schedule and operation coordinated to mitigate wind power fluctuations.

In this work, PSH and grid-scale Battery Energy Storage System (BESS) are considered to operate and smooth out wind power variability. The actual and day-ahead wind forecast data of the BPA area in 2014 is used in this work. Based on the BPA wind data, imbalance power is found from the forecasted and actual data. Imbalance power is decomposed into two separate signals (intra-day and intra-hour) to be used for HESS optimal sizing.

1.3 Predictive operation of battery energy storage with high wind penetration

Since the main obstacle of battery energy storage systems (BESS) to be implemented in the grid is the high cost of power conversion systems and batteries, optimal sizing of batteries seems essential to find the minimum size of energy storage to mitigate the intermittency of wind or solar power output. Charge/discharge or control strategy of battery energy storage directly affect the required size of power conversion system (power rating) and batteries (energy rating). Better performance of battery energy storage significantly reduces the minimum required size of batteries. In the second chapter of this thesis, a novel control method is proposed for battery energy management to fulfill a wind production commitment. This method aims to minimize the error between the day-ahead scheduled and actual production of a wind farm. The proposed strategy, basically, works based on the updated forecast data (2-hour ahead update) and a feedback from State of Charge (SOC) of the batteries to optimally manage the charge/discharge of the BESS. Also, the proposed method prevents the batteries from deep discharge and as a result, the estimated lifetime of batteries increases by using the proposed method. A new method for lifetime estimation of a battery based on rain flow cycle counting is introduced. This new method is easy to implement and requires less processing time.

The Sodium-Sulfur (NaS) type of battery is selected for simulation purposes. The results show that the new adaptive controller increases availability of the battery energy storage without decreasing its lifetime. The simulations are compared to a simple (minute-by-minute) controller. Ultimately, sizing for BESS is done in a scenario where there is a 4500 MW wind farm (BPA area), and results support the fact that a BESS with adaptive controller needs less power and energy capacity.

1.4 Optimal sizing and operation of battery energy storage systems connected to wind farms participating in electricity markets

In this chapter, the opportunities for the BESS to participate in electricity markets is reviewed. A BESS is a reliable resource to provide energy for various power system applications. The BESS can increase the flexibility and reliability of the renewable energy dispatch. Wind energy has the largest contribution among renewable energy resources and its control has become a research focus in power systems area.

In fact, the main challenge for batteries to participate in a market is the high cost. Lifetime of batteries should be estimated and modeled as a constraint in the optimization model.

A novel control strategy of a BESS is introduced thesisto increase its operating profit. An optimization problem based on RT and DA market clearing prices is developed to calculate the actual profit of the combined BESS and wind farm operation. Also, all physical and operational constraints are taken into account. Most of the papers in the literature consider the BESS as an active power source or sink. However, this thesis takes the advantage of the reactive power support of the BESS and proposes a new voltage control constraint of the coupling bus. Although there is no compensation by system operators for reactive power support at the present time, some incentives or regulations might become available in the near future for distributed energy resources. Some standards like IEEE 1547 and ANSI C84.1 require distributed generators to maintain the voltage at the point of common coupling within specified limits.

The focus of this thesis is on the maximization of the profit when the BESS is co-located with a wind farm. Thus, all related physical and operational constraints are modeled and the optimization problem is solved through a Receding Horizon Control (RHC) scheme. The

RHC require forecast of wind power and electricity price data. Therefore, wind and price data are comprehensively analyzed to obtain proper forecast models.

The word cloud of the keywords in this thesis is shown in **Error! Reference source not found.** below which is made by free online tools in wordle.net.

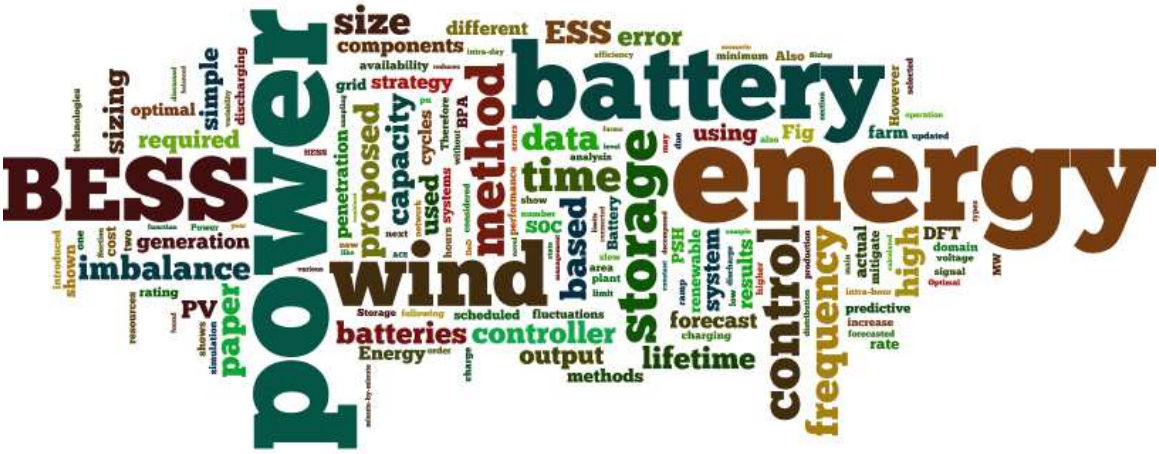

Figure 1-2 Word cloud of this thesis

CHAPTER 2: Literature Review

In this chapter, a comprehensive review on existing work is provided. The literature review in this thesis covers two main areas: planning and operation. In the first part, existing solutions on the BESS sizing is reviewed. Then, a literature review on the BESS operation is provided in the second section.

2.1 Existing work on ESS sizing

The ESS sizing can be divided into two main categories. The first category includes the methods dealing with the ESS sizing in an analytical method. The second category deals with the problem by utilizing the historical data.

In the literature, ESS sizing methods can be classified into two groups: (i) time domain approaches and (ii) frequency domain methods. Many papers have been published about ESS sizing with time domain approaches. The control strategy plays an important role in increasing the efficiency and decreasing the size of the ESS. In [10], simple, fuzzy, ANN, and advanced ANN control methods of battery energy storage are introduced and employed in time-series simulations to optimally size the BESS. Pre-compensation and post-compensation control methods to minimize hourly forecast errors are proposed in [11]. Optimal storage sizing is formulated in [12] as a stochastic linear programming problem when load and wind generation is considered as two random variables. Also, references [13] [14] [15] [16] aim at solving ESS optimal sizing problem to smooth out the variability

of wind power. In particular, [13] [14] [15] represent stochastic optimization problems to find the minimum required size of ESS with maximum operating profit while considering transmission constraints. Also, statistical analysis can be used to derive a model to predict load and wind output. In [17], a coordinated operational dispatch of Li-ion battery is studied based on a statistical analysis.

However, some papers have presented frequency domain approaches in ESS sizing. DFT method is used in [18] to decompose balancing power into real-time, intra-hour, and intra-day components. In [19], frequency domain method is used to size both battery and a diesel generator in an isolated microgrid. In [20], DFT and wavelet are used to size battery (NaS) and CAES. In this work, different aspects of using DFT and wavelet are discussed and results show that size of the HESS using DFT is smaller. Also, wavelet based method results in more wind spillage and backup energy. In [21], wavelet method is used to size an ultra-capacitor bank and a battery energy storage.

2.2 Existing work on the ESS operation

The ESS is a promising solution for any kind of intermittent renewable energy resource. Various energy storage technologies for wind power application are reviewed in [5]. Authors have compared different storage technologies from conventional (like pumped storage hydro, or PSH) to different types of BESS. Several papers are published in the literature to address aspects of renewable energy resources on future generation, and highlight technical operational issues of the grid with high penetration of variable energy resources [22] [23] [24]. In particular, small signal stability of a system with high penetration of wind turbines is discussed in [22] . In [23], the restrictions of hybrid wind and hydro storage system for connecting to the conventional grid of the Canary Islands is

investigated. A decentralized control approach for active and reactive power injection in distribution network is addressed in [24].

Gants, et al, in [25], discuss the potential improvement in reliability of distribution networks by means of distributed energy storage systems as well as distributed generations (DG). Optimal placement of energy storage systems is attempted in order to reduce societal costs of outage.

Energy storage systems can be installed to provide several services to distribution network operators including energy arbitrage, peak shaving, frequency and voltage control, outage mitigation, and distribution system equipment deferral [26], [27], [28], and [29]. Specifically, references [28] and [29] address peak shaving and energy balance applications, respectively. Reference [30] proposes a methodology to operate a battery for multiple applications. An economic dispatch problem including ancillary services, outage mitigation, and energy arbitrage are addressed and results show which service takes priority over other services.

Many control methods have been proposed in order to mitigate fluctuations. In [31], the authors develop a control methodology based on feedback-based control scheme for optimal use of the battery energy storage system.

In [32], an optimal ESS management together with a real-time control strategy is proposed where both aim to increase renewable energy penetration by means of energy buffering. Two control methods (pre-compensation and post-compensation) are introduced in [10] to minimize hourly forecasting errors. Moreover, optimal BESS sizing assessment is investigated in that paper using some new control methods. In [10], four different control methods (simple, fuzzy, ANN, and advanced ANN) of BESS are compared for large wind

turbine applications. The authors have also attempted optimal sizing of Zinc-Bromine batteries from a cost-benefit perspective to supply as much power as forecasted in preceding day. The BESS sizing problems in many of the mentioned references are presented in a system including wind turbines and a grid-scale BESS by time-series simulations.

Several studies including [33], [34], and [30] have assessed BESS economic viability and its impact on different markets. Specifically, [33] addresses technical performance and value propositions of Sodium-Sulfur (NaS) battery in NYISO and PJM markets. The BESS evaluation in CAISO market is discussed in [34]. Different services and their economic values of BESS deployment are reviewed in [30].

The studies on BESS operation can be divided into two groups: first, those that aim at improving reliability or efficiency of the power system without participating in the market [35] and [36]. Stability, reliability, security, and efficiency of power systems in transmission [37] or distribution network [38] are covered in this group.

Second, studies which consider market participation of BESS, such as [39], [40], [41], and [42]. In detail, [39] investigates benefits of BESS that is connected to a wind farm. Reference [40] introduces a framework for energy storage and demand response to optimally manage energy from demand response aggregator's perspective. On the other hand, the author in [41] and [42] study energy storage values as an independent asset. In [41], optimal bidding strategy of battery energy storage in day-ahead market is proposed. In this paper, battery as a price taker can submit bids to participate in California day-ahead market or it can be self-scheduled. Second life batteries can be a candidate of brand new batteries since they are quite cheaper but still can produce energy but for less duration. Using

the used or second life batteries in grid scale operation is also considered in [41]. A similar problem with a larger BESS while participating as a price-maker is addressed in [42].

Self-scheduling problem, basically, comprises an objective function (for example the profit that should be maximized) and couple of technical and physical constraints. In [43], a method for self-scheduling of individual pumped storage hydro is proposed to participate in energy and reserve (spinning reserve) market. At the end of self-scheduling time span, energy stored in upper reservoir is checked to have the same energy level prior to the start time of self-scheduling. In [44], self-scheduling of pumped storage hydro in energy and reserve market (spinning and frequency regulation market) with simplified technical constraints is addressed. A heuristic self-scheduling method with composition of Hydro plant and PSH in a competitive electricity market is proposed in [45]. Self-scheduling of PSH and NaS battery is formulated in [46]. In this thesis, co-optimization of energy and reserve in electricity market for both PSH and battery is addressed to economically compare profitability of batteries and PSH in electricity market. Authors showed traditional technologies like PSH has more economical merits than emerging technologies. However, in modern power grid with higher renewable energy penetration, demands for more fast-acting energy storages like batteries is increasing. The fast fluctuation of renewable energy resources calls for fast regulation up/down among ancillary services.

In [47], a structure for self-scheduling of PSH to increase the profit for integrated operation of wind and PSH is introduced. Planning and operation of combined wind power and pumped storage is addressed in [48], [49], [50]. In these papers, it is assumed that wind farm owner should must pay for energy storage, which is not realistic, and individual energy storages can participate in electricity and reserve market.

Authors, in [51], seek find an optimal operation of individual owned battery energy storage in energy and reserve market in a market similar to PJM

An optimal real-time energy management for the BESS is introduced in [52] to increase the RES penetration. In [10], ANN and fuzzy control methods of the BESS are developed to mitigate wind power fluctuations and meet DA commitments. Reference [11] aims at minimizing the hourly forecast errors by introducing two control methods (pre-compensation and post-compensation) to fulfill hour to hour commitment. Both [10] and [11] study optimal sizing of the BESS by means of long-run time series simulations. On the other hand, authors in [53] and [54] utilize probabilistic wind forecasts in their models to develop a RHC for the BESS to minimize the hourly scheduling errors.

Few papers consider high-resolution information of the market to increase the profitability of the BESS. A forecast model to detect price spikes in the RT market is proposed in [55]. The forecast model is utilized in an optimization problem to increase the BESS profit while operating in Ontario's electricity market.

CHAPTER 3: OPTIMAL SIZING OF HYBRID ENERGY STORAGE SYSTEMS TO MITIGATE WIND POWER FLUCTUATION

3.1 Introduction

High renewable energy penetration levels may be adversely impacted by frequency deviations as a result of wind power fluctuations. Energy Storage System (ESS) can be a viable candidate for mitigating wind power fluctuations. However, economic considerations for ESS may cause significant limits in implementation. Therefore, effectiveness and optimal size of ESS are important to study. This chapter addresses methods to find an optimal size of sodium sulfur or Li-Ion battery energy storage to mitigate PV fluctuations. Two different methods for optimal sizing are introduced in the first section of this chapter. Also, a novel method for sizing of BESS and pumped storage hydro is proposed, in the second section of this chapter, to accommodate high penetrations of wind energy. The proposed method decomposes the imbalance power by using Discrete Fourier Transform (DFT) to fast and slow components. Hence, different ESS technologies can be dispatched based on their effectiveness in various time spans. For instance, the slower pumped storage hydro can compensate slow cycles, and the fast-acting batteries can be dispatched to balance smaller and more frequent cycles. This method can be used in the planning of different ESS technologies. The schematic of this method is presented in Figure 3-1. Comparative studies on real wind data from Bonneville Power Administration (BPA) shows the efficacy of the proposed method.

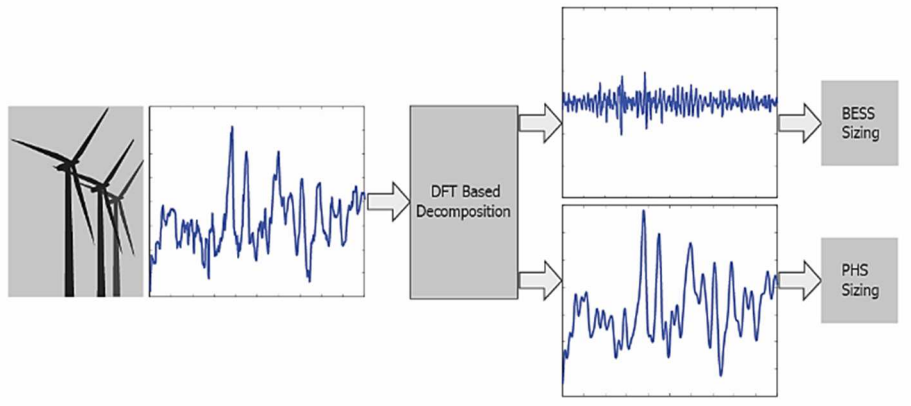

Figure 3-1 Imbalance power decomposition schematic.

3.2 Time Domain Approaches

Each battery energy storage needs the power rating based on Power Conversion System (PCS) capacity and energy rating based on size of the batteries. In time domain approaches, energy and power ratings are calculated based on analysis is carried or simulation is performed in time domain. Generally speaking, there are two methods to find the optimal size of the battery energy storage system:

- Analytical method based on worst case scenario
- Simulation method based on control strategy

In this part, the application of PV in finding the minimum size of batter is considered. It is worth noting that the requirements for size of the battery storage associates with:

- Capacity of PV plant
- Field size of PV plant (dimensions)
- Average and worst rate of fluctuations (average and high cloud speed based on historical data)

- Acceptable ramp rate limit due to limits of grid interconnection

3.2.1 Analytical method based on 90% power drop/rise

In this scenario, it is assumed that the BESS is sized to support one worst fluctuation cycle. This fluctuation is dropping from 100% to 10% PV generation equal to 90% of nominal PV capacity. This method guaranties the best power sizing but it slightly underestimates the energy ratings. The reason would be because this method ignores the fact that PV generation can slowly rise without any charging of batteries and another significant fluctuation happens after a while and there is no energy stored in batteries to support the grid. More than that, it doesn't take the charging/discharging efficiencies. The analytical method results in fully discharge of batteries; however, the recommended operational SOC is 30%-80% and this fact should be considered, too.

Maximum PV generation reduction (increase) in a windy and cloudy day depends on the speed of wind and the geographical dimensions of the PV plant. The faster the clouds move, the faster the PV power falls (rises). Also, in a bigger PV plant, it takes more time for the land to be covered fully by clouds. The power drop of PV production can be explained with an exponential function based on a time constant [56]. Figure 3-2 illustrates how exponentially PV power production falls. In this figure also the expected ramp rate limit is shown. Battery energy storage can be good candidate to balance the deficit between ramp rate limit and actual power drop.

In the following figures, the concept of 90% PV power drop and rise is depicted. The maximum/minimum of BESS output is the required inverter size and the hatched area shows the required energy capacity for a battery to mitigate PV fluctuations.

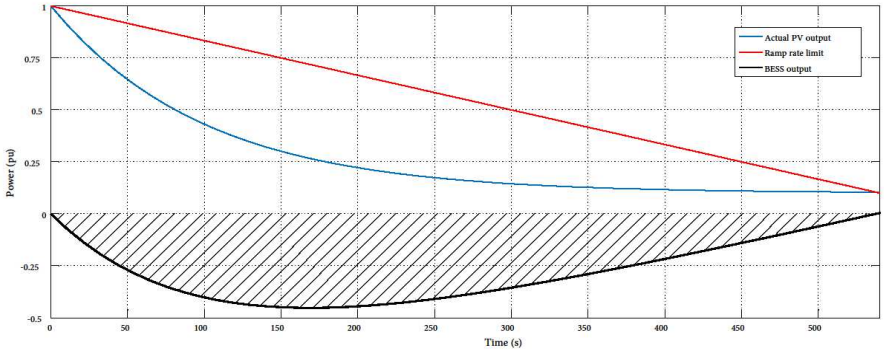

Figure 3-2 Output power of PV vs ramp rate limit and the required battery output to mitigate the PV power drop. Hatched area shows energy required to fulfill the ramp rate limit.

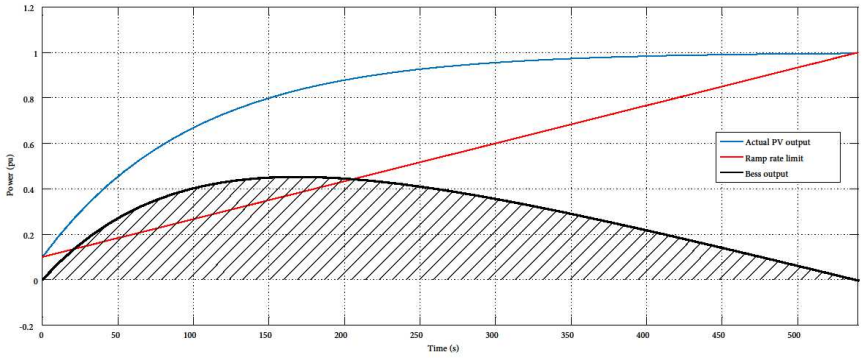

Figure 3-3 Output power of PV vs ramp rate limit and the required battery output to mitigate the sudden PV power rise.

P_{BES} at each time can be derived as:

$$P_{BES}(t) = ramp.\mathrm{t} - P_{PV} \tag{3.1}$$

$$P_{PV} = 90e^{-t/\tau} + 10 \tag{3.2}$$

Where τ is time constant for the exponential function in second and is defined as follows [56]:

$$\tau = \frac{\sqrt{a.b}}{v} \tag{3.3}$$

Where

a, b Length and Width of the plant (m)

v Wind speed (m/s)

Then P_{BES} can be written as:

$$P_{BES}(t) = \frac{P_{PV}^{r}}{100}\left(100 - ramp.\frac{t}{60} - \left(90e^{-t/\tau} + 10\right)\right) \tag{3.4}$$

Where

$P_{BES}(t)$ Battery power (KW)

P_{PV}^{r} PV plant power capacity (KW)

τ Cloud coverage time constant (s)

$r_{\max}$ Ramp up/down limit (%/min)

Maximum required power capacity of the inverter can be found by maximizing the above function.

$$\frac{dP_{BES}(t)}{dt} = \frac{P_{PV}^{r}}{100}\left(-ramp/60 + 90/\tau e^{-t_{\max}/\tau}\right) = 0 \tag{3.5}$$

$$t_{\max} = \tau \ln\left(5400/\tau.ramp\right) \tag{3.6}$$

By plugging (3.6) into (3.4) maximum value of P_{BES} can be found:

$$P_{rated} = \frac{P_{PV}^{r}}{100}\left[90 - \tau.ramp\left(1 + \ln\left(\frac{5400}{\tau.ramp}\right)\right)\right] \tag{3.7}$$

Where

P_{rated} is power rating (KW) of inverter.

The energy function can be found by taking the integral of the power function. Suppose T_s is the time that the PV output reaches 10% of the nominal power, then $E(t_s)$ would be the maximum energy required to firm PV output fluctuations.

$$T_s = \frac{5400}{ramp} \tag{3.8}$$

$$E_{rated} = 2.\int_0^{T_s} P_{BES}(t) \tag{3.9}$$

Note that, to cover both rising and falling fluctuations, twice the calculated energy rating is considered.

$$E_{rated} = \frac{0.9P_{PV}^{r}}{1800}\left[\frac{2700}{ramp} - \tau - \tau.e^{-5400/\tau.ramp}\right] \tag{3.10}$$

In the following figures, it is shown that a higher size of PV plant results in a smoother drop of PV output. Consequently, the required power and energy ratings for the BESS in smaller PV plants are relatively higher than larger PV plants.

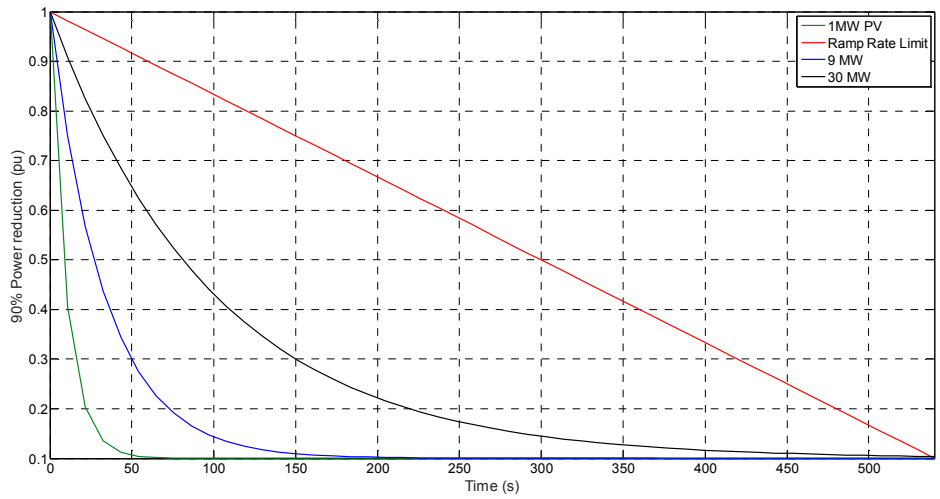

Figure 3-4 Correlation between size of PV plant and speed of power drop.

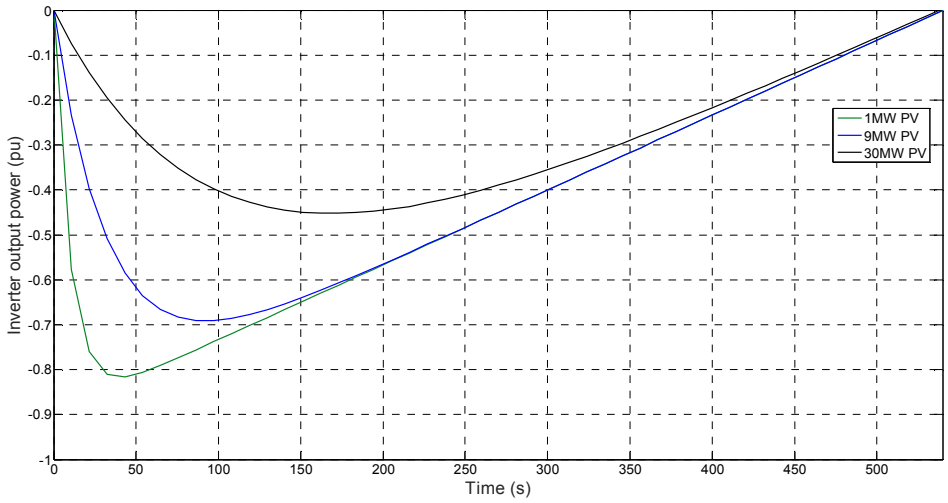

Figure 3-5 Correlation between size of PV plant and the relative size of BESS.

The geographical area of 1 MW PV power plant in the Marshal power plant (operated by Duke Energy) is 10500m^2. One can estimate the size of a 9 MW PV power plant by scaling from 1 MW. Also, 40 MPH is considered as high wind speed which is quite an overestimate for 95% of the time in a year. For a 9 MW solar plant with 10% ramp rate control, the power rating can be calculated by plugging the given numbers in (3.7):

$$P_{rated} = 6500\,KW \tag{3.11}$$

Using the same numbers gives the energy ratings for batteries:

$$E_{rated} = 1000\,KWh \tag{3.12}$$

Please note that, this size of battery is to support the worst PV generation fluctuation. However, it needs some maneuverability for more fluctuation and charge/discharge losses. This size of battery results in SOC=0% at lowest energy level and SOC=100% at the highest energy level. Double the size (2000KWh) may be needed to utilize half of the battery energy capacity to stick with 0.3<SOC<0.8 limit.

3.2.2 Simulation method based on control strategy

The size of the energy storage highly depends on the requirements from the grid side and the control strategy for charging/ discharging from the inverter side. Most o utilities prefer smooth power injection from PV plant; however, due to unpredictable nature of the solar irradiance, battery energy storage needs to be involved to make sure the PV fluctuations doesn't affect the stability of the power grid. One of the main requirements from the grid side is to receive energy within a ramp rate limit. It means if the fluctuations doesn't violate the ramp rate, the power injection from the PV plant is good enough. Otherwise, the battery should inject or absorb power to smooth out the power fluctuations and bring the combined power to the required standard.

In this part, the simple ramp-rate control is implemented, and the optimal size of the battery and inverter from the power output of BESS can be found. This method should be able to validate the analytical method's results. The schematic of the block diagrams for ramp-rate control is presented in Figure 3-6.

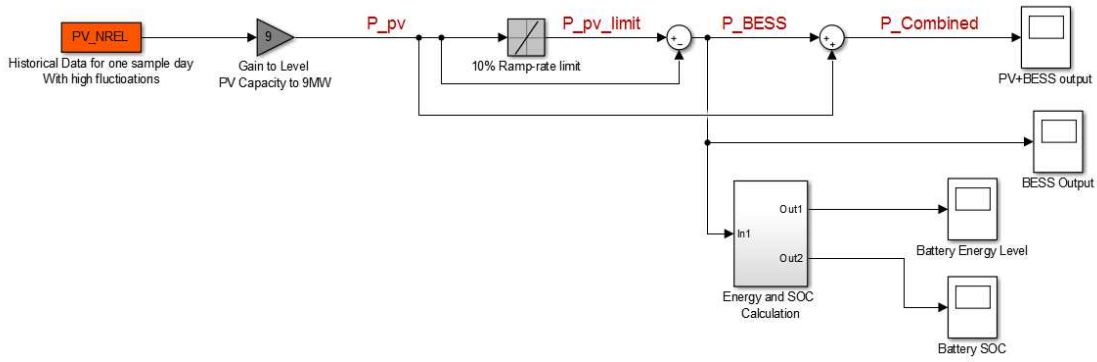

Figure 3-6 Schematic of ramp rate control.

The results for combined output, BESS output, Battery energy level, and Battery SOC is shown in Figure 3-7.

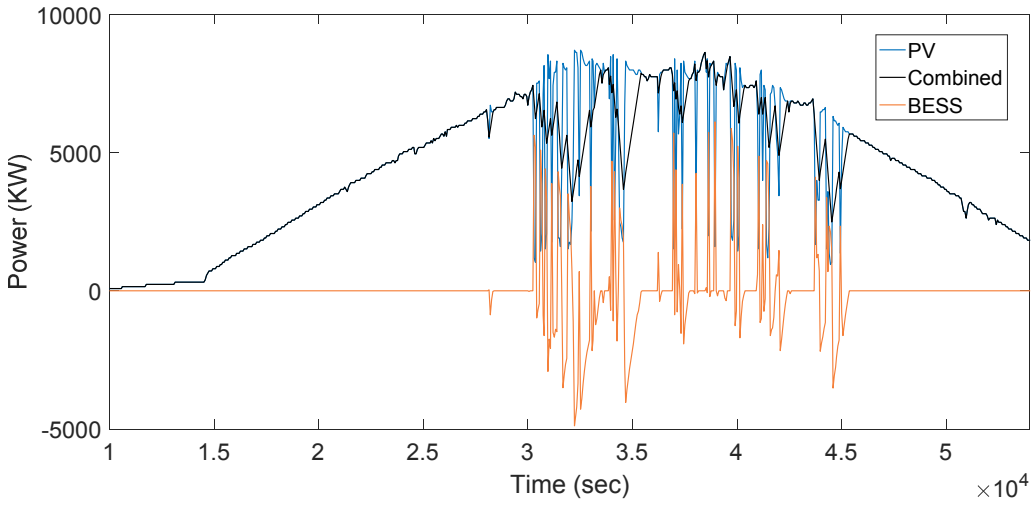

Figure 3-7 PV output for a day with a high fluctuations, BESS output, and combined PV and BESS output.

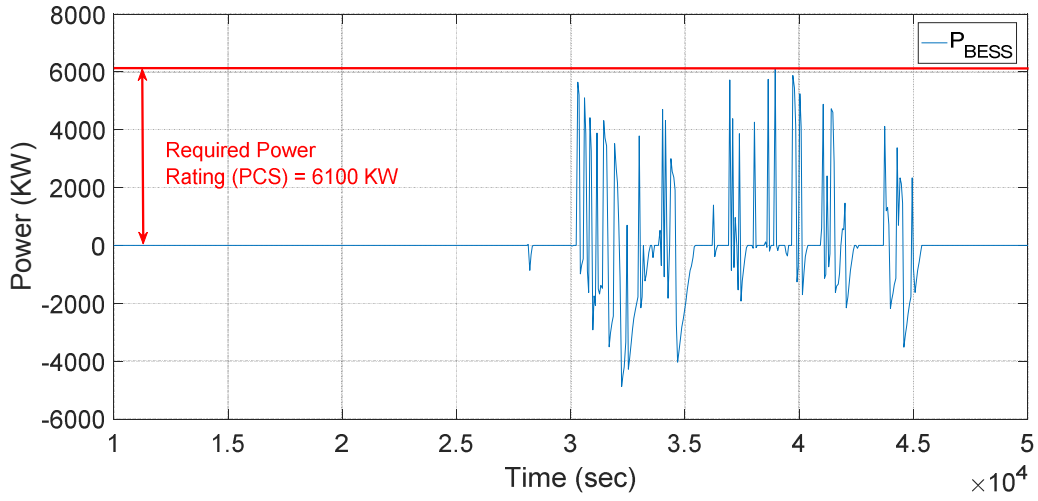

Figure 3-8 Finding the minimum power capacity from BESS output in a cloudy day.

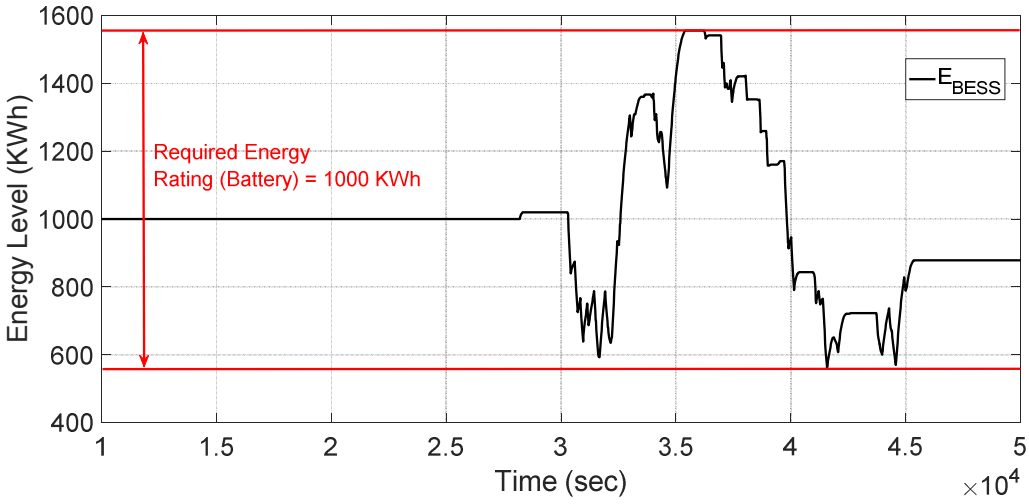

Figure 3-9 Finding the minimum energy rating from energy level of BESS in one cloudy day.

Simulation results are close to the analytical results. To observe the SOC changes, E=2000KWh is selected and the results show that SOC remains between 30% and 80% and the deeper discharges doesn't occur.

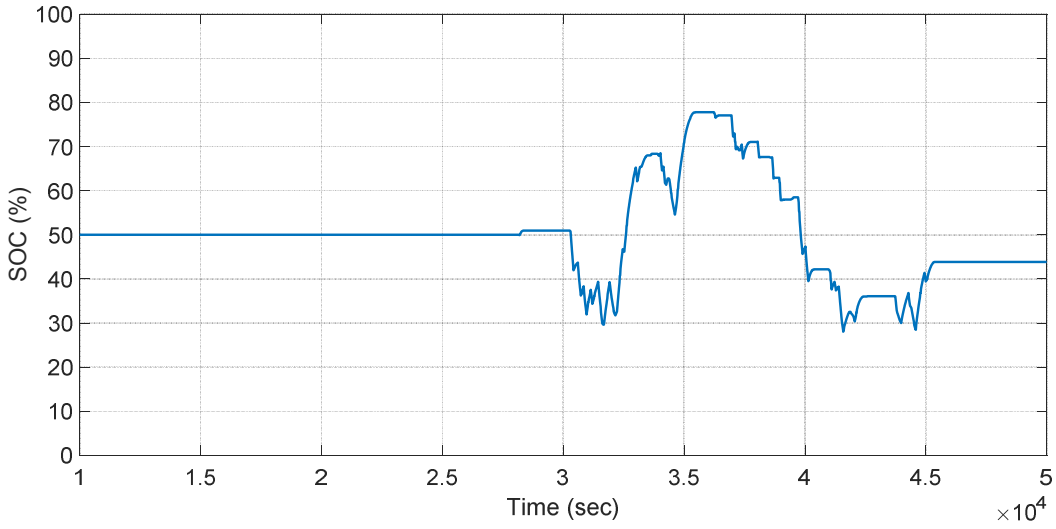

Figure 3-10 SOC track of battery for one day for 2000 KWh batteries

3.3 Frequency Domain Approaches: Sizing of Two or More ESS

Different ESS technologies have different response times. For example, batteries are fast responding equipment suitable for variety of applications, from frequency response to spinning reserves. However, the slower ESS are just suitable for applications which do not require fast-acting technologies (e.g. spinning reserve). In this section, a new method based on DFT is proposed to decompose the balanced error between the scheduled power and the actual wind power and assign to the slower PSH and the faster BESS. The schematic of this process is depicted in Figure 3-1.

3.3.1 System Modeling

Energy storage systems are being used in power systems with high penetration of renewable energy resources. The key role of ESS is to smooth wind power fluctuations to allow higher penetration of wind power in the system.

Imbalance power (also known as forecast error) of a wind farm without ESS at any time can be defined by:

$$P_{Sch}(\mathrm{t}) - P_{Wind}(\mathrm{t}) = P_{imbalance}(\mathrm{t}) \tag{3.13}$$

Where $P_{Sch}(\mathrm{t})$ is scheduled wind power based on 1-day ahead forecast for sample point t, $P_{Wind}(\mathrm{t})$ is actual wind generation of wind farms at sample point t, and $P_{imbalance}(\mathrm{t})$ is the imbalance power.

In order to increase penetration of wind generation in a power system, imbalance power should be minimized. Adding energy storage helps to mitigate the imbalance. The ESS injects energy when scheduled wind power is more than actual wind power and absorbs energy to store the excess generation.

$$\begin{cases} P_{Sch}(t) > P_{Wind}(t) \Rightarrow P_{imbalance}(t) > 0 \Rightarrow ESS\ sources \\ P_{Sch}(t) < P_{Wind}(t) \Rightarrow P_{imbalance}(t) < 0 \Rightarrow ESS\ stores \end{cases} \tag{3.14}$$

Figure 3-11 shows the imbalance power in 2014 for the BPA area. Actual wind generation and one day-ahead forecast data of BPA for different years can be found in [57].

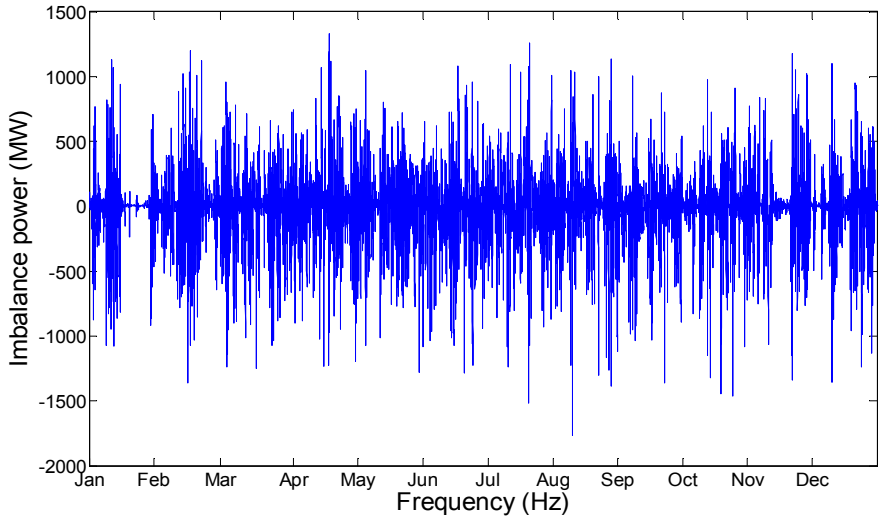

Figure 3-11 Forecast error of BPA in 2014.

3.3.2 DFT Analysis

DFT transforms equally spaced data into the coefficients of sinusoids which are ordered by their frequencies. The imbalance power can be decomposed into different frequency components by DFT. Different parts of a signal can be formed by slow and fast cycles. Low frequency signal represents intra-day errors and it corresponds to the slow PSH operation. Also, high frequency signal, which represents intra-hour errors, commands BESS operation. In this work, DFT is utilized to decompose imbalance data for the course of one year to determine required power and energy capacity that should be injected or absorbed. Therefore, DFT can be used in planning level for HESS sizing. It can be used for HESS operation as well. Imbalance power can be estimated based on updated forecast data for the window of 2-4 hours. Estimated imbalance power can be decomposed into high and low frequency components to command BESS and PSH.

$$X_k = \sum_{t=0}^{N-1} x[t].e^{\frac{-i2\pi kt}{N}},\ k = 0,1,...,N-1 \tag{3.15}$$

$$x[t] = \frac{1}{N}\sum_{t=0}^{N-1} X_k . e^{\frac{i2\pi kt}{N}} \quad , t = 0,1,...,N-1 \tag{3.16}$$

where N is the number of sample data. DFT of a signal returns N components with different frequencies listed in monotonically increasing frequency order. The real parts in the Fourier transform of a signal are mirrored over half of the data points. In other words:

$$X_k = X^*_{N-k} \quad 1 < k < N-1 \tag{3.17}$$

Where operator (*) represents conjugation. Also frequency resolution is:

$$f_r = \frac{1}{NT_s} \tag{3.18}$$

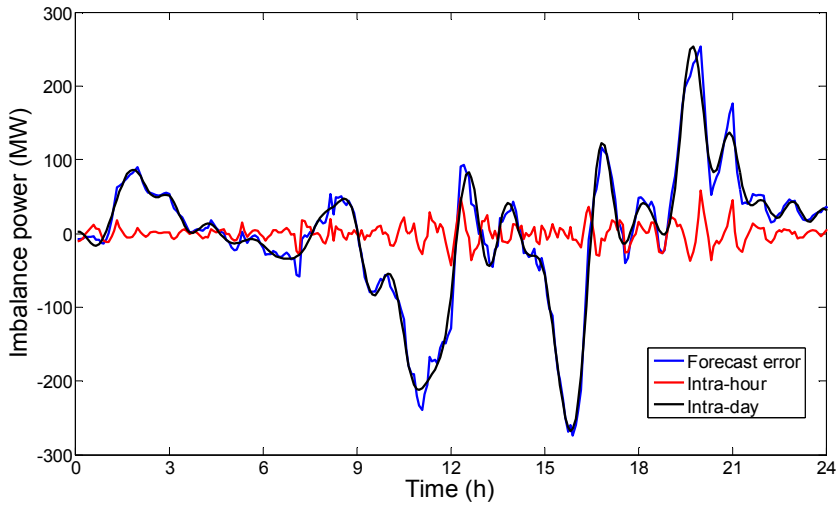

Figure 3 -12 Imbalance power for a sample day in March 2014.

where f_r is frequency resolution and T_s is the time interval of data points in seconds.

As mentioned earlier, actual wind and forecast data for BPA area in 2014 is used in this work. Since time intervals for the data are 5 minutes, the number of sample data for the

whole year (N) is 105,120, sampling frequency f_s is 33e-4 Hz, and frequency resolution is 3.2e-8 Hz.

3.3.3 HESS Sizing Algorithm

In this section, power (MW) and energy (MWh) sizing of two energy storage systems are discussed. First, two signals with high and low frequency components should be found from the imbalance power signal. Then, each signal is used to obtain an appropriate size of each ESS. The algorithm to determine the assigned power for BESS and PHS is shown below:

Algorithm for Applying DFT

1- Find imbalance power ($P_{imbalance}$(t)) for 1 year using (1).
2- Find the Fourier transform of imbalance power as discussed in the previous section.
3- Use the high pass and low pass filters (based on desired cut-off frequencies) to extract high frequency and low frequency components.
4- Take inverse Fourier transform from high-frequency and low-frequency signals to bring them back into time domain.
5- Assign $P_{e,hf}(t)$ to BESS where high frequency components correspond to BESS and assign $P_{e,lf}(t)$ to PSH as slow cycles correspond to PSH.

The forecast error with its intra-hour and intra-day components for a day in March 2014 in the BPA area is shown in Figure 3 -12. After acquiring intra-hour and intra-day components, they can be used for power and energy sizing of HESS.

A. Power sizing

Minimum power capacity required to minimize imbalance power for BESS and PSH can be found from the following expressions:

$$P_{BESS} = \max\left\{\left|P_{e,hf}(t)\right|\right\}$$
$$P_{PHS} = \max\left\{\left|P_{e,lf}(t)\right|\right\} \tag{3.19}$$

Where

$P_{e,hf}$ high and medium frequency components of imbalance power

$P_{e,lf}$ low frequency components of imbalance power

P_{BESS} rated power of BESS (MW)

P_{PHS} rated power of PSH (MW)

Typically, some reserve capacity for ESS should be considered to take care of unforeseen prediction errors of wind energy. This contingency concern, however, is not the focus of this thesis.

B. Energy Sizing

For determining energy capacity of BESS and PSH the following steps should be followed:

Step 1) Find the maximum and minimum accumulative energy function of decomposed signals.

$$E_{acc,hf}(t) = \int_0^t P_{e,hf}(t)\,\mathrm{dt}$$
$$E_{acc,lf}(t) = \int_0^t P_{e,lf}(t)\,\mathrm{dt} \tag{3.20}$$

For 5-min interval data points, the above equations can be converted to:

$$E_{acc,hf}(t) = \sum_{m=0}^{t}\left(P_{e,hf}(m).\frac{5}{60}\right)$$
$$E_{acc,lf}(t) = \sum_{m=0}^{t}\left(P_{e,lf}(m).\frac{5}{60}\right) \tag{3.21}$$

Step 2) Determine SOC limits of BESS.

$$SOC_{low} < SOC < SOC_{up} \tag{3.22}$$

Where SOC_{low} and SOC_{up} are, respectively, minimum and maximum limits of the state of charge. In this chapter, SOC_{up} for both BESS and PSH is selected 1 and SOC_{low} is 0.1 and 0 for BESS and PSH, respectively.

Step 3) Find the minimum energy storage for each signal (intra-day and intra-hour) from the following expressions:

$$E_{BESS} = \frac{\max\left\{\left|E_{acc,hf}(t)\right|\right\} - \min\left\{\left|E_{acc,hf}(t)\right|\right\}}{SOC_{up} - SOC_{low}}$$
$$E_{PHS} = \max\left\{\left|E_{acc,lf}(t)\right|\right\} - \min\left\{\left|E_{acc,lf}(t)\right|\right\} \tag{3.23}$$

3.4 Simulation Results

A spectrum analysis was done on the DFT of the 2014 wind speed imbalance data from BPA area. It is worth mentioning that frequency domain components will be sorted in frequency order. However, data points should be scaled in Hz by using (3.18). Spectrum analysis of forecast errors are shown in Figure 3-13 and Figure 3-14. Data in the frequency domain is mirrored over half of the sampling frequency. Hence, low and high pass filters are designed symmetrically as depicted in Figure 3-15 and Figure 3-16. Table 3-1 contains specifications of frequency bands of the imbalance power.

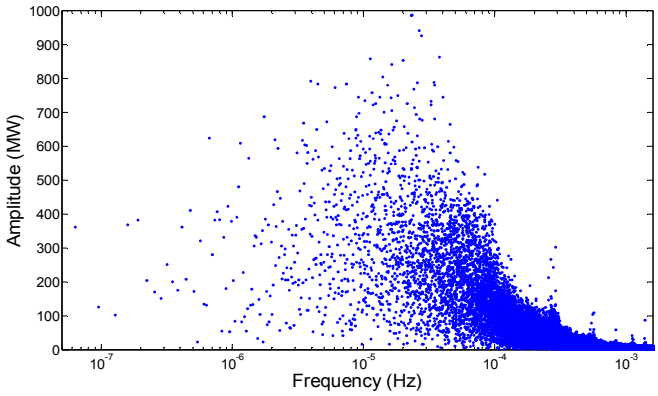

Figure 3-13 Frequency spectrum dot density map.

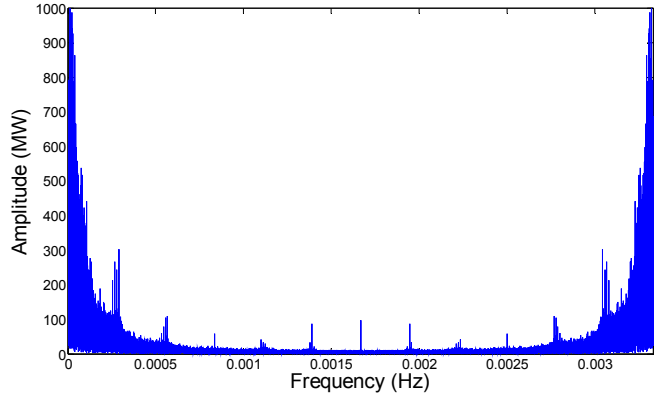

Figure 3-14 Frequency spectrum curve.

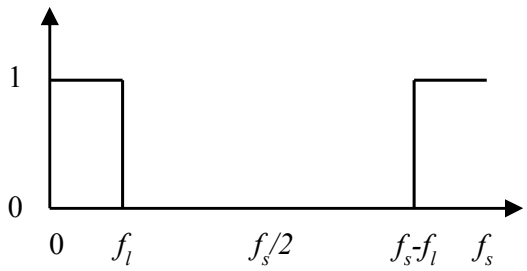

Figure 3-15 Low pass filter schematic.

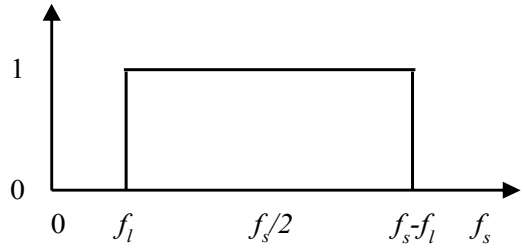

Figure 3-16 High pass filter schematic.

Table 3-1

Specifications of Various Components of Imbalance Power

Component	Technology	Response time	Cut-off Frequencies [fl fu]
Intra-hour	BESS	10 minutes to 1 hour	[2.78e-4 0.0017]
Intra-day	PHS	1 hour to 12 hours	[2.31e-5 2.78e-4]

Typically, batteries can be used as a fast-acting energy storage and their response times are less than a minute. Nevertheless, in this work, the fastest response time of the battery is

limited to 10 minutes due to Nyquist-Shannon sampling theorem. According to the theorem, frequencies higher than half of the sampling frequency ($0.5f_s$) cannot correctly be returned to time domain. Since imbalance power is decomposed into two signals, one cut-off frequency is enough, which is 2.78e-4 Hz. Slow components with bigger amplitude on the left hand side of the red line are assigned to PSH and smaller and more frequent components (right hand side of the red line) are linked to BESS.

Power capacity (MW), energy capacity (MWh), efficiency, lifetime, capital cost, and ramp up/down rate are characteristics of energy storage technologies. Hybrid energy storage configuration is done in this chapter based on power and energy capacity. Efficiency, state of charge limits, and ramp up/ down limits are also considered in the HESS configuration. A NaS type of battery is selected for BESS with 15% loss during charging/discharging. When BESS is suitable for small fluctuations, PSH (with extremely high-energy capacity) is chosen to compensate slow cycles. Typical PSH ramp up/down rate is 100 MW/min and maximum ramp rate required in the simulation is 70 MW/min.

Intra-hour and Intra-day signals are obtained by using inverse DFT of filtered components. Figure 3-17 and Figure 3-18 show intra-hour and intra-day imbalance power for the whole year of 2014 in the BPA area.

Maximum intra-hour imbalance power is 760 MW. Considering 85% efficiency of battery, power capacity of BESS is 894 MW. Energy capacity is also obtained by (3.23). The energy rating of BESS along with power and energy ratings of the PSH is listed in Table 3-2. Also, required power and energy sizing for imbalance power shown in Figure 3-17 is provided in Table 3-2 (single configuration). In other words, by using a single ESS technology

(without considering ramp rate and efficiency), 1765 MW power and 25.3 GWh is required to entirely balance the forecast error.

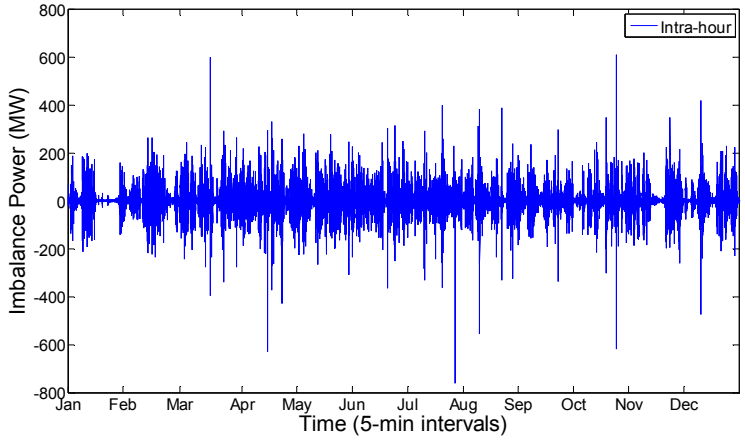

Figure 3-17 Intra-hour imbalance power for 2014 in BPA area

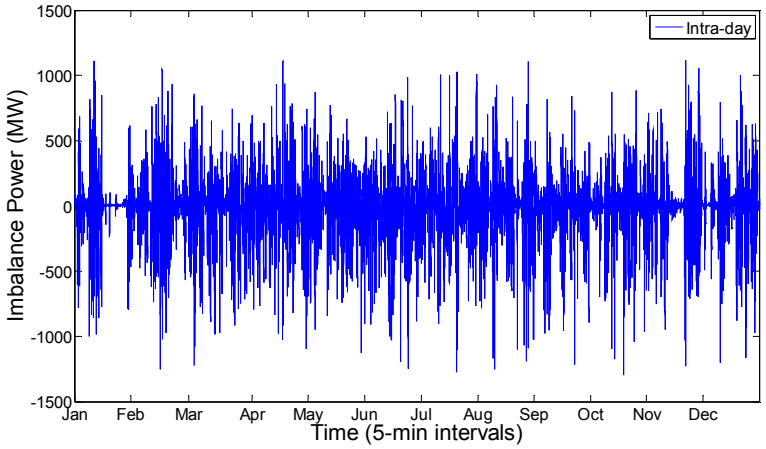

Figure 3-18 Intra-day imbalance power for 2014 in BPA area.

Table 3-2

BESS and PHS sizing results

Configuration	Technology	Power	Energy
Hybrid	BESS	784 MW	132 MWh
	PHS	1,297 MW	22.7 GWh
Single	BESS or PHS	1,765 MW	25.3 GWh

Nevertheless, some of the intra-hour errors seem off from the average, and they occur infrequently. Since the capital cost of the battery is so high, these errors can be ignored and it's not cost-effective to keep the main portion of the power conversion systems (PCS) for some errors that happen only a few times in a year. Hence, it may be concluded that the reduced power rating of the battery may be enough to mitigate most of the errors. Figure 3-19 shows that a 200 MW inverter (instead of 798 MW) mitigates more than 95% of the errors.

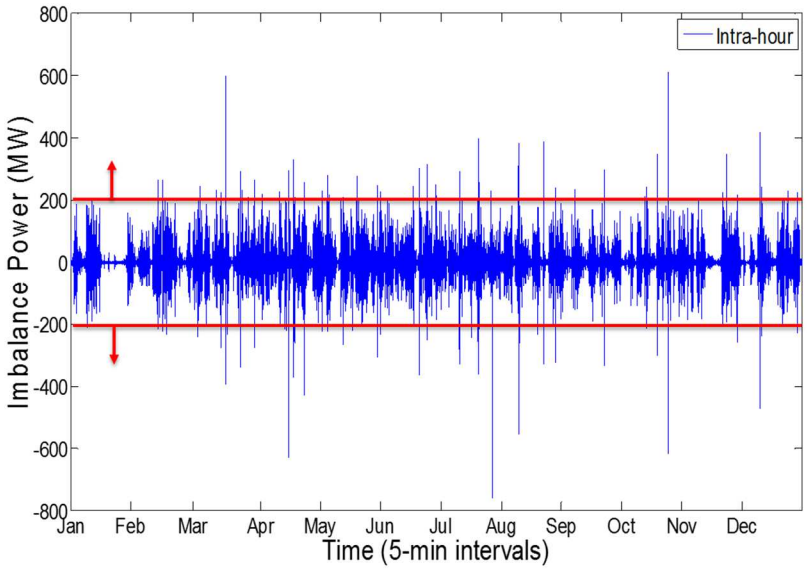

Figure 3-19 Intra-day imbalance power for 2014 in BPA area.

PSH has a ramping limitation of 100 MW/5-min. Therefore, 30 minutes for ramping from idle time to maximum power generation would be enough. One can move the cut-off frequency (switch time between PSH and BESS) to see what the required sizes for batteries and PSH are. It is insightful to see the trend of the required capital cost by changing the switch time between PSH and BESS. The following capital cost is assumed:

$$C_{ESS} = \left(K_E^{BESS} E_{rated}^{BESS} + K_P^{BESS} P_{rated}^{BESS} + K_E^{PSH} E_{rated}^{PSH} + K_P^{BESS} P_{rated}^{BESS}\right)$$
$$\begin{cases} K_E^{BESS} = 0.4 \ \$/Wh \\ K_P^{BESS} = 0.2 \ \$/W \end{cases} \quad \begin{cases} K_E^{PSH} = 0.1 \ \$/Wh \\ K_P^{PSH} = 0.2 \ \$/W \end{cases} \tag{3.24}$$

Figure 2.20 shows the tradeoff between capital cost and switching time. It seems that changing from 40 minute to 80 minutes does not dramatically change the capital cost.

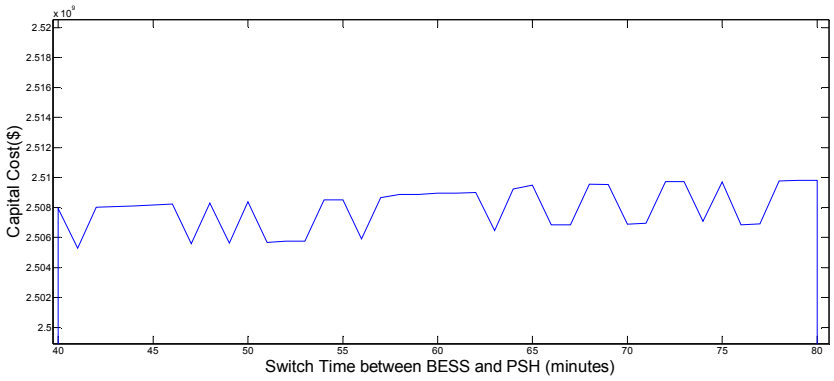

Figure 3-20 tradeoff of capital cost by changing the switching time

3.5 Conclusion

In this Chapter, different methods for sizing of energy storage systems have been addressed. The requirements for BESS to mitigate adverse effects of high PV penetration were reviewed in the first part of this chapter. Next, two methods to find the minimum power and energy required by the grid are addressed. The analytic method is based on the

worst case scenario when PV generation drops (rises) 90%. Simulation of ramp rate control shows the trend of charging and discharging for a BESS connected to a PV plant. NREL historical data was used for simulation purposes.

Then, a hybrid configuration of energy storage systems was proposed to mitigate wind energy fluctuations. Capital cost of energy storage systems is the main obstacle for them to be deployed. Much research has been conducted to increase efficiency and decrease the required size of ESS. Some types of ESS (like batteries) can respond rapidly and are suited to mitigate high frequency components of imbalance power. However, some other types of ESS are more efficient for slow cycles. DFT based method is used to break out slow and fast components of imbalance power. By using high and low pass filters, frequency domain signal of imbalance power is decomposed and is transformed to the time domain by inverse DFT. In this chapter, a DFT-based coordinated strategy is introduced to distribute power between BESS and PSH. A methodology to determine power and energy capacity of each type of ESS is discussed. To validate the effectiveness of the proposed method, actual data of BPA for 2014 is used in the simulations.

CHAPTER 4: PREDICTIVE CONTROL OF BATTERY ENERGY STORAGE WITH HIGH WIND ENERGY PENETRATION

4.1 Introduction

High penetration of wind energy requires fast-acting dispatchable resources to manage energy imbalances in the power grid. Battery Energy Storage Systems (BESS) are considered an essential tool to decrease the power and energy imbalance between the scheduled generation (day-ahead forecast) and the actual wind farm output. The control methodology or battery management strategy greatly impacts the performance of the energy storage system. Better performance of the BESS reduces the minimum required size of batteries for wind variability mitigation. This thesis proposes a novel control method for BESS to fulfill a production commitment. This method, called 'predictive controller' is based on updated forecast data to improve the performance of the energy storage system and consequently reduce the required size of the BESS. The Sodium-Sulfur (NaS) type battery is selected for simulation purposes. Results show that the predictive controller reduces the error (between scheduled generation and actual wind farm output) more than the simple method (also known as the minute-by-minute method) and other proposed methods in the literature. Also, a new formulation for the battery lifetime estimation is introduced, and it is used to analyze the impact of the proposed method on the battery lifetime depreciation. The schematic of the co-located BESS and wind farm is illustrated in Figure 4-1.

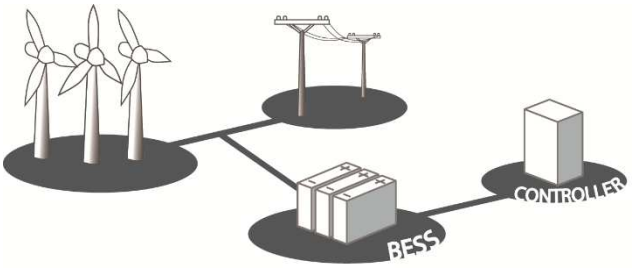

Figure 4-1 Combination of BESS and wind farm

Optimal sizing of the BESS is about selecting the minimum required size of the battery to allow the combined output power (BESS and wind turbines) to match a day-ahead scheduled (forecasted) power within a tight tolerance (e.g. ±5% error for 90% of the time). This criterion depends on the size of the wind farm and the characteristics of the connected network. A novel battery management strategy is introduced in this thesis. It is based on a predictive scheme to manage charging, discharging, and idle modes so as to increase the flexibility of the system to keep the energy balanced between the generation and the demand. Battery charging/discharging strategies directly affect sizing requirements for a hybrid power system with wind and energy storage. Therefore, the size of the battery can be reduced with a better battery management strategy without compromising the quality of performance. A battery control method is a key factor in life-time analysis. To be more precise, in a specific operational and environmental situation, battery control algorithm plays a crucial role in increasing/reducing battery lifetime. In this thesis, the lifetime of a battery energy storage system is estimated to evaluate the performance of the proposed control method and ensure that it does not degrade battery lifetime. Most of the proposed control methods of BESS in the literature decrease battery lifetime to even less than affected by the simple (or minute-by minute) controllers. Therefore, the contributions in this chapter can be summarized as follows:

- A novel control strategy for battery energy storage based on updated forecasted data is proposed. This increases availability of the battery in the long run to ensure meeting the reserve commitments in various scenarios.
- The proposed method minimizes the required size of the battery for a specific system. In this work, optimal sizing of the battery is determined and compared with the existing research to show the effectiveness of the proposed control method.
- Lifetime estimation based on cycle counting is used to evaluate the impact of the proposed method on battery degradation. Results show that the predictive control method, unlike other existing control methods, does not reduce the expected lifetime of the battery and it works as well as a simple controller. However, using the proposed method results in a higher range of availability, rather than the simple controller.

In contrast with [31] and [52], the focus of this work is on the control of the BESS to increase the balanced energy in a minute-to-hour timeframe. Hence, the focus is not on the power quality of the battery output. As a result, this work is partially comparable with [10]-[11].

This chapter is organized as follows. The combined wind farm and BESS power balance formulation and BESS modeling are presented in Section II. Simple (minute-by-minute) controller and the proposed predictive controller are introduced in Section III. Simulation results are discussed in Section IV and conclusions are presented in Section V.

Let us introduce the following nomenclatures for this chapter:

Indices

k, T Time step and horizon time

LI Life index in lifetime estimation algorithm

n Number of total cycles

Variables and Parameters

P_{rated}^{B} BESS rated power

E_{rated}^{B} BESS rated Energy capacity

C_p Power conversion costs

C_E Battery cost

η_c, η_d Charge and discharge efficiencies

η_d' Auxiliary parameter for discharge efficiency

K Control Coefficient

L_{BESS} Battery lifetime in years

CF Number of cycles to failure at specific Depth of Discharge (DoD)

Time Series Data

$P^{W}(k)$ Wind turbines output power

$SOC(k)$ BESS state of charge

$P^{B}(k)$ BESS output power

$P^{Sch}(k)$ Scheduled wind power generation (1-day ahead forecasted wind output power)

$P_{error}^{Sch}(k)$ Scheduling error (difference between 1-day ahead forecasted output and actual wind farm output)

$P_{error}(k)$ Final error or difference between 1-day ahead predicted output and combination of wind farm and BESS

$\hat{P}^{W}(i \mid k)$ Estimated forecast of wind for time *i*, issued at time *k*

$\hat{E}_{error}(k+T \mid k)$ Estimated energy deficiency or excess for next *T* time step, issued at time *k*

All power and energy units in this thesis are in per unit.

4.2 Problem Statement for Predictive Control of BESS

The main purpose of using BESS in conjunction with a large wind farm is to mitigate wind power fluctuations. Although there are no incentives for wind farm owners to install BESS, there will be some constraints with increased renewable energy penetration. In this chapter, it is assumed that there is a constraint, which only allows the error between the wind farm output and the day-ahead forecasted power to be within a specific limit. Discussions on this constraint are covered in section III.

In the first part of this section, modeling of a wind farm combined with BESS is discussed.

4.2.1 System Modeling

The typical combination of wind farms with battery energy storage is shown in Figure 3-1. Power balance of a wind farm without BESS referring to the generic K^{th} sampling time can be expressed as:

$$P_{error}^{Sch}(k) = P^{Sch}(k) - P^{W}(k) \tag{4.1}$$

By adding a BESS, Eq. (4.1) can be improved as follows:

$$P_{error}(k) = P^{Sch}(\mathrm{k}) - P^{W}(k) - P^{B}(k) \tag{4.2}$$

Generally speaking, the objective of adding grid size energy storage is to have the minimum error between predicted output and actual wind farm output. Therefore, energy storage should either compensate for energy shortage or store any extra wind energy that would otherwise be curtailed.

$$\begin{aligned} & P_{error}(k) = 0 \\ & \Rightarrow P^{B}(k) = P_{error}^{Sch} = P^{Sch}(\mathrm{k}) - P^{W}(k) \end{aligned} \tag{4.3}$$

It is worth noting that $P^{B}(k)$ is negative when battery sinks (charging mode) and positive when battery sources energy into the grid (discharging mode).

$$\begin{cases} P^{Sch}(\mathrm{k}) > P^{W}(k) \Rightarrow P^{B}(k) > 0 \\ P^{Sch}(\mathrm{k}) < P^{W}(k) \Rightarrow P^{B}(k) < 0 \end{cases} \tag{4.4}$$

Figure 4-2 shows information and power flows between wind turbines, grid, and BESS.

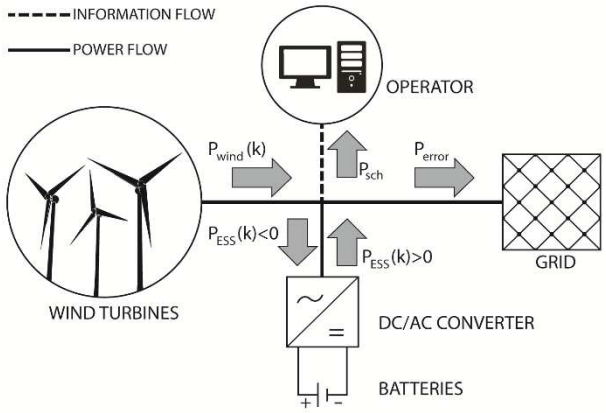

Figure 4-2 Interaction of BESS with network, operator, and wind farm

4.2.2 BESS Modeling

Many papers about BESS modeling have been published to include battery and inverter characteristics. For example, reference [58] investigates stability analysis of converter-connected BESS. In this thesis, a simple modeling of BESS without any filter and static

compensator is addressed, whereas this work focuses on battery charging/discharging management; power quality is not a concern at this stage.

The battery state of charge (SOC) can be derived as follows:

$$\mathrm{SOC(k)} = \mathrm{SOC(k-1)} - \frac{\eta(k-1)\cdot K \cdot P^{B}(k-1)}{12E^{B}_{rated}} \quad \text{and} \quad \eta(k) = \begin{cases} \eta_c & P^{B}(k) \le 0 \\ \eta'_d = 1/\eta_d & P^{B}(k) > 0 \end{cases} \tag{4.5}$$

$$SOC^{\min} \le \mathrm{SOC(k)} \le SOC^{\max} \tag{4.6}$$

Note that η_c and η_d denotes charging and discharging efficiencies, respectively. In the case of NaS, η_c is 85% and η_d is 87% [10]. In this work, an auxiliary parameter (η'_d) is used instead of η_d for the sake of simplifying the above equations. Equation (4.5) shows that SOC of a battery at each time depends on initial SOC and amount of energy injected or withdrew from the battery during the last time interval. The 1/12 factor in (4.5) is due to the 5-minute sample time of the time series data.

It is worth noting that the efficiency of batteries is not constant, it varies with current flow, temperature, state of charge, etc. For instance, due to internal resistive losses in batteries, the efficiency improves when current goes down and it deteriorates with higher current. In this thesis, $SOC^{\min}$ and $SOC^{\max}$ are 0.2 and 0.9, respectively.

Note that per unit values are used for all power and energy variables because it will be easier to scale the size of BESS for different wind farms. More discussions on per unit and absolute values are provided in section IV. Charging and discharging constraints, imposed by battery and inverter limitations, are described in Equation(4.7).

$$P_{ESS}(\mathrm{k}) = \begin{cases} 0 & SOC = 0 \,\&\, P_{ESS}(\mathrm{k}) > 0 \\ 0 & SOC = 1 \,\&\, P_{ESS}(\mathrm{k}) < 0 \\ 0 & SOC < \eta_d . P_{ESS}(k) \big/ 12E_{rated} \\ 0 & (SOC - 1) > \eta_c . P_{ESS}(k) \big/ 12E_{rated} \\ P_{rated} & P_{ESS}(\mathrm{k}) > P_{rated} \,\&\, SOC \neq 0 \\ -P_{rated} & P_{ESS}(\mathrm{k}) < -P_{rated} \,\&\, SOC \neq 1 \\ P_{ESS}(\mathrm{k}) & else \end{cases} \tag{4.7}$$

These constraints simply imply that batteries cannot have any power output when $SOC(k) = SOC^{\min}$, and cannot charge when the battery state of charge is full ($SOC(k) = SOC^{\max}$). The third limitation in equation (4.7) describes that BESS cannot source power into the grid when the commanded power is more than the energy that remains in the battery. Similarly, the fourth constraint does not let BESS get charged to more than its capacity. The fifth and sixth constraints state that the output or the input power of BESS cannot exceed its rated power.

4.2.3 Battery Lifetime Estimation

In most types of batteries, lifetime and performance highly depend on the depth of discharge (DoD) of charging/ discharging cycles. Also, there are some environmental factors (like temperature and humidity) that affect the battery's performance. Accurate analysis of battery lifetime and its chemical degradation requires prolonged laboratory experiment verification, which is not the focus of this work.

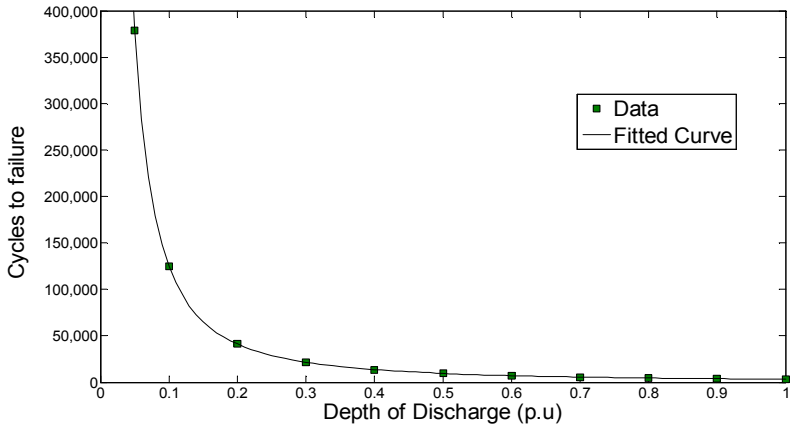

Figure 4-3 Number of cycles to failure at each DoD for NaS battery (data from [34]).

Nonetheless, DoD of cycles and SOC limits are two manageable factors in control algorithms. Although accurate lifetime analysis of batteries is not the focus of this work, a lifetime estimation based on cycling numbers and depth of discharge is described. In order to estimate battery lifetime, the DoD of each cycle and the total number of charging/ discharging cycles in a specific time should be counted. Consequently, the battery lifetime can be estimated as follows [34]:

$$L_{BESS} = \frac{T}{\sum_{i=1}^{m} \frac{N_i}{CF_i}} \tag{4.8}$$

where T is the duration of simulation in years, CF_i is the number of cycles to failure at corresponding DoD, Ni is the number of cycles at each DoD, and m is number of DoD ranges. The number of cycles to failure for each DoD is shown in Figure 3-3. Based on 10 data points provided in [59], a curve is fitted and a model for CF_i is extracted in Figure 4-3.

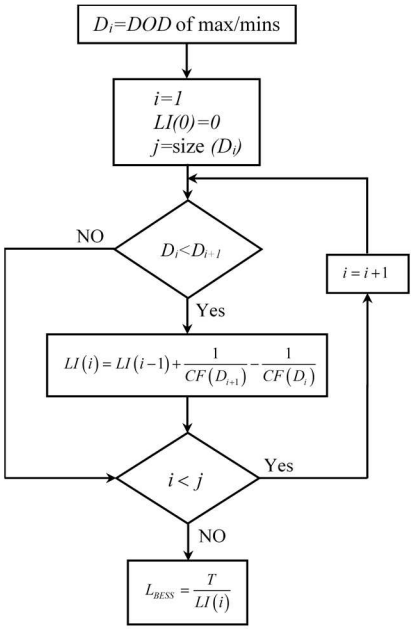

Figure 4-4 Lifetime estimation algorithm based on cycles counting and calculating equivalent lifetime for incomplete cycles.

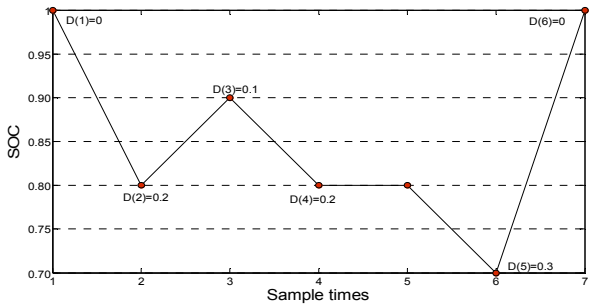

Fig 3- 1 An example to show incomplete cycles and finding DoD from SOC diagram.

It worth mentioning that the DoD in Figure 4-3 represents depth of discharge of complete cycles. Due to wind farm output variability, the BESS switches between charging/discharging modes frequently. Therefore, in real operations, more incomplete cycles happen. Various methods of cycle counting are addressed in [11], [59] , and [60]. In this section, a simple algorithm for battery lifetime modeling based on cycle counting is developed. The flowchart in Figure 4-4 shows how to simply estimate battery life depreciation.

The flowchart in Figure 3-4 shows how to simply estimate battery life depreciation for different charging/ discharging curves. *LI* is an auxiliary accumulative index that corresponds cycles to failure, and L_{BESS} is an estimated lifetime of battery based on cycles curve. The algorithm aims at estimating a battery's lifetime using a battery's SOC diagram which is recorded for a specific time (*T*). Local min/maxes of the SOC diagram is found. Then, according to the flowchart, a vector comprising DoD of the local max/mins is constructed. Initial values are set and *LI* is calculated and updated in the loop. Iterations are stopped when the last point in the SOC diagram is reached and then L_{BESS} is calculated. In order to illustrate the concept of the flowchart, a sample SOC diagram is depicted in Figure 4-8. Also, six local min/maxes (e.g. $j=6$) with associated D_i values are shown in this figure.

In order to better understand the concept, one has to know what the complete cycle means. When a discharge starts from full State of Charge (meaning SOC=1), and it follows with a full charge back to SOC=1, one may call it a complete cycle. Otherwise cycles are considered as incomplete. There are some references showing how an incomplete cycle can be written as subtraction of two complete cycles. Our battery lifetime estimation algorithm calculates equivalent complete cycles in order to estimate battery degradation. To elaborate the idea, refer to the example in Figure 4-8. This SOC trend can be decomposed into two different trends.

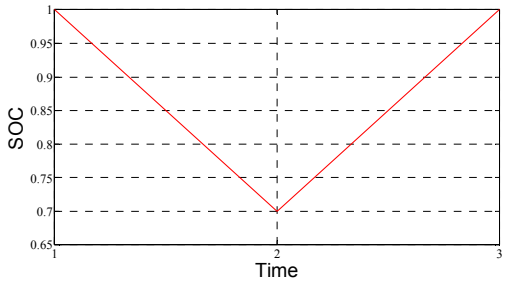

Figure 4-5 Example of complete cycle [0.7-1]

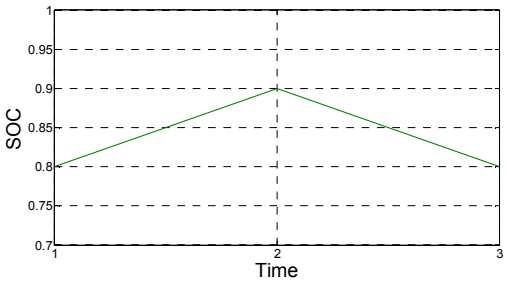

Figure 4-6 Example of incomplete cycle [0.8-0.9]

Let us define cycle [a-b] as follow:

Cycle [a-b] means that a variation in SOC starts from point a, increases/decreases to reach point b, and returns to point a.

If a or b is equal to one, the cycle would be considered as a complete cycle. Otherwise, the cycle would be incomplete.

Incomplete cycle [0.8-0.9] is equal to incomplete cycle [0.9-0.8] for battery lifetime calculations.

According to [61], one can calculate incomplete cycles:

Incomplete cycle [0.8-0.9]= incomplete cycle [0.9-0.8]= complete cycle[0.8-1] – complete cycle[0.9-1]

Therefore, Fig. 3-5 can be converted to:

Total cycles= Complete cycle [0.7-1] + complete cycle [0.8-1] - complete cycle [0.9-1]

Also, note that current rate (power rate) may impact some types of batteries. The current rate is interpreted as the DoD divided by the cycle duration. Two complete cycles with similar DoD and different current rates are depicted in the following figure:

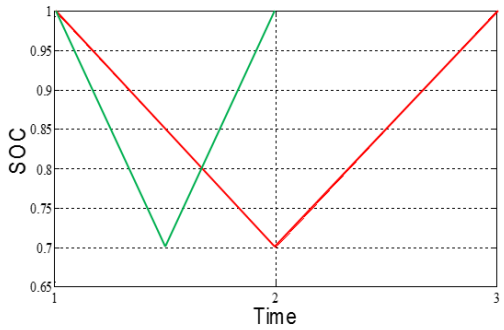

Figure 4-7 Two different SOC trends: One with higher current rate (green) and the other one with lower current rate (red)

The green cycle has a higher current rate than the red cycle for charge and discharge. Lithium-ion is relatively sensitive to the current rate and its lifetime depends not only on the DoD, but also on the current rate [62]. However, the NaS battery is not sensitive to the current rate and thus, it was not considered in the formulations and algorithm presented in the thesis.

In order to estimate the battery's lifetime, one needs to find complete cycles. However, in most cases, one may not see complete cycles in the SOC diagram of a battery. Suppose, there is an SOC diagram like Figure 3-5. One may use the lifetime estimation algorithm presented in Figure 3-4. Different steps of the algorithm are explained in the following statements:

a- According to the first block from the top, a vector that includes the DoD of max/mins is constructed. In other words, the local min /maxes of SOC diagram (e.g. Figure 4-8) are found. Then, the correlated DoD are easily calculated.

$$D_i = \begin{bmatrix} 0 \\ 0.2 \\ 0.1 \\ 0.2 \\ 0.3 \\ 0 \end{bmatrix}$$

b- In the second block, set *i=1*, *LI=0*, and *j=6*. Let us introduce *LI* as an auxiliary variable to simplify our calculations.

c- Then, move forward to the loop.

i=1

1- Is D_2 greater than D_1? Yes. Go to the next block.

2- *LI(1)=LI(0)+1/CF(0.2)-1/CF(0)*

Suppose *CF(0.2)* ≅ *45,000* and *CF(0)=inf* which can be found from Figure 4-3.

3- Is i<j? Yes. Increment i and go to step 1 and repeat.

i=2

1- Is D_2 greater than D_1? No. Go to step 3.

3- Is i<j? Yes. Increment i and go to step 1 and repeat.

i=3,4,5, and 6 is omitted for brevity.

d- After 5 iterations, L_{BESS} can be found from below:

$$L_{BESS} = \frac{T}{LI(i)}$$

Where *T* is the time of simulation in year. For example, if Figure 4-8 is the trend of SOC and it is repeated every 12 hours, L_{BESS} can be obtained from the following:

$$L_{BESS} = \frac{1/2/365}{1/CF(0.2) + 1/CF(0.2) - 1/CF(0.1) + 1/CF(0.3) - 1/CF(0.2)} = \frac{1.37e^{-3}}{1/45e^{3} - 1/12e^{4} + 1/3e^{4}} = 29\,(years)$$

4.2.4 Cost-benefit Analysis

The following cost model represents the capital cost of the BESS with consideration of battery cells and power conversion system.

$$\begin{aligned} &Cost = C_P.P_{rated} + C_E.E_{rated} \\ &\begin{cases} C_P = 0.22 \ \ (\$/W) \\ C_E = 0.35 \ \ (\$/Wh) \end{cases} \end{aligned} \tag{4.9}$$

This cost model does not include installation and O&M. Costs of power conversion system and battery cells are selected based on some papers (like [4]- [5]) and some manufacturer prices.

The wind farm combined with the BESS is paid for providing energy, based on Market Clearing Price (MCP), in addition to the tax return and federal credits. It is assumed that wind turbines can curtail the wind excess, and the penalty for deviation is just applied for wind energy deficiency. The BESS gains profits as follows:

1- During the excess of wind power, the BESS would get charged and this allows the investor to collect the tax return and federal credits for the absorbed energy by the BESS. Also, charging with the excess of wind means that the BESS investor does not need to pay for energy in the real-time market, based on Locational Marginal Prices (LMP).

2- During the wind energy deficiency, the BESS would be paid for the delivered energy based on day-ahead MCP together with the tax return and federal credits.

4.3 Control Algorithm

Frequency is typically controlled through three different steps: primary control, secondary control, and tertiary control. The generator governors, the frequency responsive loads, and fast acting energy storages (like flywheel and some types of batteries) are

responsible for primary control of the second-to-second power mismatch. In this chapter, the focus is on compensating imbalance error in a minute-to-hour timeframe. Satisfying (4.3) in the presence of high penetration of variable energy resources requires a large amount of reserves. The balancing authority computes the Area Control Error (ACE) in an area from (4.10). This utilizes contingency reserves to minimize the error [63].

$$ACE = (T_a - T_s) - 10\beta(f_a - f_s) \tag{4.10}$$

Where T_a is actual interchange power in MW, T_s is scheduled interchange power in MW. f_a and f_s represent actual and scheduled frequency, respectively. Also, β is the frequency bias constant in MW/0.1Hz.

The main purpose of adding the BESS is to minimize the ACE which meets the requirements imposed by authorities. For instance, the North American Electric Reliability Corporation (NERC) enacted the Balancing Area ACE Limit (BAAL) as a short term ACE metric [64]. Changing rate of second term in ACE calculation is less than the first term (T_a-T_s). Therefore, it can be inferred from Equation (4.10) that there is no need for a complete match between scheduled power and actual power to have zero ACE, because actual frequency is also a key factor in ACE calculation. Severity of frequency deviations caused by power mismatch highly depends on the characteristics of the connected power system. The main concern of this work is to increase the availability of the battery to reduce the imbalance error for most of the times power mismatch happens. ±5% error for 90% of the time as the strict criteria is selected in this chapter for simulations. However, this criteria may be modified with respect to the connected system's structure and characteristics.

In this section, minute-by-minute or simple controller is introduced, and then, a novel predictive control strategy is proposed.

4.3.1 Minute-by-minute Control

Minute-by-minute or simple controller is a typical controller type in existing BESS (minute-by-minute and simple controller can be used interchangeably). This controller does not require any additional information.

Battery energy storage system will sink to the grid if the error between 1-day ahead forecasted power (scheduled power) and actual wind generation exceeds 0.05 per unit. Likewise, the BESS will charge if the wind generation exceeds the scheduled power by 0.05 per unit. Since there is no penalty for scheduling errors between (-0.05, 0.05), no action for BESS is required for this mismatch.

$$P_{ESS} = \begin{cases} 0 & \left|P_{Error}^{Sch}(k)\right| < 0.05 \\ P_{Error}^{Sch}(k) & \left|P_{Error}^{Sch}(k)\right| > 0.05 \end{cases} \tag{4.11}$$

Currently, renewable energy is traded in electricity market even if wind farms produce more than their scheduled power.

However, as renewable energy gains higher penetration, new standards and market policies will likely be issued in order to maintain the stability and reliability of the network.

4.3.2 Predictive Control

As shown in (4.3), the total output error will be zero if $P^{B}(k)$ is equal to $P_{error}^{Sch}(k)$. However, in many cases, due to lack of wind power generation, the battery discharges all its energy into the grid, in which case, the battery gets depleted and cannot provide more energy.

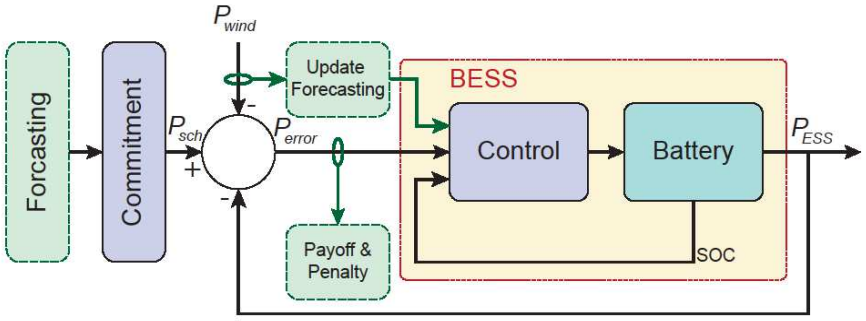

Figure 4-8 Predictive control schematic

Therefore, the corresponding bus voltage will drop leading to additional issues. To overcome this problem and to maintain the bus voltage within 0.95 and 1.05 per unit, the BESS rate of charge/ discharge should be managed better. To put it differently, the BESS should be allowed to discharge into the grid to adjust the voltage of connected bus back to the range [0.95-1.05] pu. Based on network configurations and specifications, this charging/ discharging rate may differ. Therefore, a criteria on $P_{error}(k)$ should be defined based on the characteristic of the connected network. In this chapter, 5% error of power is chosen for simulation.

It is not possible to optimally manage BESS charging/ discharging, unless there is some information about wind production in the following hours. Updating forecasted data allows BESS to observe the wind profile for the next few (2 ~ 3) hours, known as prediction horizon, and then compare them with 1 day-ahead data. Predictive control in this thesis is based on receding horizon, which repetitively solves a control problem using prediction of future states of variables, constraints, and disturbances over a moving time horizon. The basic concept of this predictive control is shown in Figure 4-9. At each time step, the control problem is solved over a fixed time horizon, and the first control input from this horizon is

applied. At the next step, the prediction horizon is shifted and the same procedure is repeated.

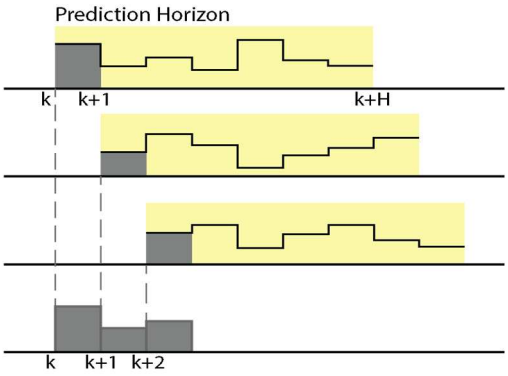

Figure 4-9 Model predictive scheme using receding horizon

If the required energy for the next few hours is more than the energy capacity of BESS, the controller should reduce the output power of BESS to save some energy for the next time steps. The BESS output can be restrained by a control coefficient (K) which as shown in (4.12):

$$P^{B}(k)=\begin{cases}0 & \text{if error is small } (\left|P_{error}^{Sch}(k)\right|<0.05)\\ P_{error}^{Sch}(k) & \text{enough energy in battery}\\ K.P_{error}^{Sch}(k), 0\le K\le 1 & \text{not enough energy in battery}\end{cases} \qquad (4.12)$$

Abundance or shortage of energy for the next 2~3 hours can be calculated by using updated predicted data. This calculation can be done every 5, 10, or 20 minutes depending on the update intervals. More updates give more precise forecast about the future wind profile and wind generation. Based on the calculated energy for the next few hours, *K* can be defined at each time step to save energy as much as possible. This controller uses minute-by-minute strategy for the usual times when the charge of the battery is enough for the next few hours. The schematic of the proposed method in a block diagram is depicted in Figure

4-10. Note that, the "payoff and penalty" block does not provide a direct feedback to the controller. However, this block can be used in an economic assessment of the BESS.

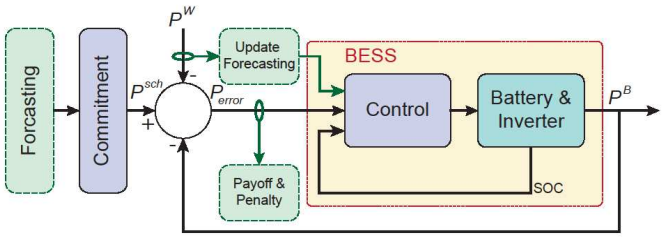

Figure 4-10 Block diagram of using predictive control in wind production commitment. The controller uses SOC, updated wind data, and the error between the scheduled power and the combined wind and BESS output power.

To decide whether BESS should limit its discharge rate, a variable should be defined, as follows:

$$\hat{E}_{error}(k+T\mid k)=\frac{\sum_{i=k}^{k+T-1}\left(P^{Sch}(i)-\hat{P}^{W}(i\mid k)\right)}{12} \tag{4.13}$$

The 1/12 factor in (4.13) is used because of the 5-minute sampling time of the time series data. Please note that the 1/12 factor should be modified for other sampling times. The algorithm for the controller is shown as follows:

Algorithm (run every 5 minutes):

1- Calculate $\hat{E}_{error}(k+T\mid k)$ for the next two hours

2- Calculate SOC(k)

3- If $P_{error}^{Sch}(k)>0$ $\Rightarrow$Discharge:

   a. $\hat{E}_{error}(k+T\mid k)<(E_{rated}^{B}\cdot SOC(k))$

      $\Rightarrow P^{B}(k)=P_{error}^{Sch}(k)$

b. $\hat{E}_{error}(k+T \mid k) > (E^{B}_{rated} \cdot SOC(k))$

$\Rightarrow P^{B}(k) = K_{d} \cdot P^{Sch}_{error}(k)$

4- If $P^{Sch}_{Error}(k) < 0 \Rightarrow$Charge:

a. $\hat{E}_{error}(k+T \mid k) > 0$

$\Rightarrow P^{B}(k) = P^{Sch}_{error}(k)$

b. $\hat{E}_{error}(k+T \mid k) < -(E^{B}_{rated}(1-\mathrm{SOC(k)}))$

$\Rightarrow P^{B}(k) = K_{c} \cdot P^{Sch}_{Error}(k)$

In order to find the best possible battery management strategy, *K* should be calculated based on the power mismatch between scheduled generation and the availability of the wind for the next predictive horizon (2~3 hours). At any time interval, it can be assumed that there is either an abundance or a shortage of wind energy in the upcoming prediction horizon. Therefore, there is either charging or discharging for the rest of the horizon. This assumption is acceptable, because if wind generation fluctuates up and down around the scheduled generation, the BESS would easily handle the fluctuations and it would not require calculating *K*. The main problem happens when there is a shortage (or abundance) of wind generation for the entire prediction horizon. Consequently, the battery is fully discharged (or charged) before the end of the horizon. In this case, the controller should manage the stored energy by calculating and applying *K*. First, it is assumed that there is a shortage of wind generation and the BESS should discharge. According to (4.5), the state of charge can be written for various time steps as shown in (4.14):

$$\begin{aligned} SOC(k+1) &= SOC(k) - \frac{\eta_d' \cdot K_d \cdot P^B(k)}{12E^B_{rated}} \\ SOC(k+2) &= SOC(k+1) - \frac{\eta_d' \cdot K_d \cdot P^B(k+1)}{12E^B_{rated}} \\ &\vdots \\ SOC(k+T) &= SOC(k+T-1) - \frac{\eta_d' \cdot K_d \cdot P^B(k+T-1)}{12E^B_{rated}} \end{aligned} \tag{4.14}$$

By summing the above equations together, many terms cancel out and (4.15) can be derived.

$$SOC(k+T) = SOC(k) - \frac{\eta_d' \cdot K_d}{12E^B_{rated}} \sum_{i=k}^{k+T-1} P^B(i) \tag{4.15}$$

Assuming full discharge of BESS in T time step periods yields:

$$if\ \ SOC(k+T) = 0.2 \Rightarrow K_d = \frac{12 \cdot (SOC(k) - 0.2) \cdot E^B_{rated}}{\eta_d' \cdot \sum_{i=k}^{k+T-1} P^B(i)} \tag{4.16}$$

Note that K_d is assumed to be constant at each time step and should be recalculated in the next time step. Equation (4.16) has a term that includes K_d in itself. Hence, equation (4.17) can be derived from (4.3) as:

$$\sum_{i=k}^{k+T-1} P^B(i) = K_d \sum_{i=k}^{k+T-1} P^{Sch}_{error}(i) \tag{4.17}$$

Finally, K_d can be calculated by applying (4.17) in (4.16):

$$K_d = \sqrt{\frac{12 \cdot SOC(k) \cdot E^B_{rated}}{\eta_d' \left(\sum_{i=k}^{k+T-1} \left(P^{Sch}(i) - \hat{\mathrm{P}}^W(i \mid k) \right) \right)}} \tag{4.18}$$

By using η instead of η_d' and setting final SOC in the horizon equal to the maximum allowable SOC ($SOC(k+T)$=0.9), a similar expression can be derived for the charging scenarios:

$$K_c = \sqrt{\frac{12 \cdot \left(SOC(k) - 0.9 \right) \cdot E^B_{rated}}{\eta_d' \left(\sum_{i=k}^{k+T-1} \left(P^{Sch}(i) - \hat{\mathrm{P}}^W(i \mid k) \right) \right)}} \tag{4.19}$$

The calculation for charging scenario is omitted for brevity. Needless to say, the square root expression remains positive, since both numerator and denominator are negative.

4.4 Simulation Results and Discussions

It is assumed that a BESS is combined with a large wind farm to mitigate variability of wind output. One simulation scenario is considered with the aim of showing effectiveness of the proposed control method. For this scenario, an arbitrary power and energy capacity is used. In the second and third parts of this section, optimal sizing and lifetime estimation of the battery is covered.

The results are compared to the performance of a minute-by-minute controller, and the probability of balanced energy of each control strategy is calculated. The persistence model forecasting with some modification is used for updated predicted data. Actual wind production and one day-ahead forecast data with 5-min intervals for the year 2013 is used for the simulation. The installed capacity of wind power in Bonneville Power Administration (BPA) territory in 2013 was 4.5 GW [65].

Note that per unit values are used in this thesis simplicity in scaling the solution. Thus, 4.5 GW wind capacity at BPA is taken as the base value to convert all wind data ($P^W(k)$) into per unit. However, absolute values can be used in all formulations. In this case, P^B_{rated} should be W, kW, or MW and E^B_{rated} should be Wh, KWh, or MWh, respectively. Also, sampling intervals should be in hours. $T = 24$ is selected which shows that the forecast period for the predictive controller is 2 hours. Needless to say, each hour has 12 time steps due to the 5-minute sampling time.

4.4.1 Sample Scenario ($P^{B}_{rated} = 0.15pu, E^{B}_{rated} = 0.55pu$)

Simulations for one year's worth of actual wind data are performed for three separate cases: (i) no BESS, (ii) BESS using predictive control, and (iii) BESS using a simple controller. Figure 4-11 shows the histogram of P_{error}, which demonstrates the probability of various errors. Results show that 23% of wind production is out of the range of ±0.05 pu error without using BESS. However, devoting the simple controller reduces the out of range error probability (±0.05 pu) to approximately 9% and the predictive control method can bring the error probability down to 7%. Therefore, it can be inferred that the selected battery reduces the imbalance error by 13.5% using the simple control strategy, and by 12% using the proposed method. Hence, with the same size of the battery, one may reach around 12% improvement with only a better control strategy. The sample period of discharging scenario is shown in Figure 4-12.

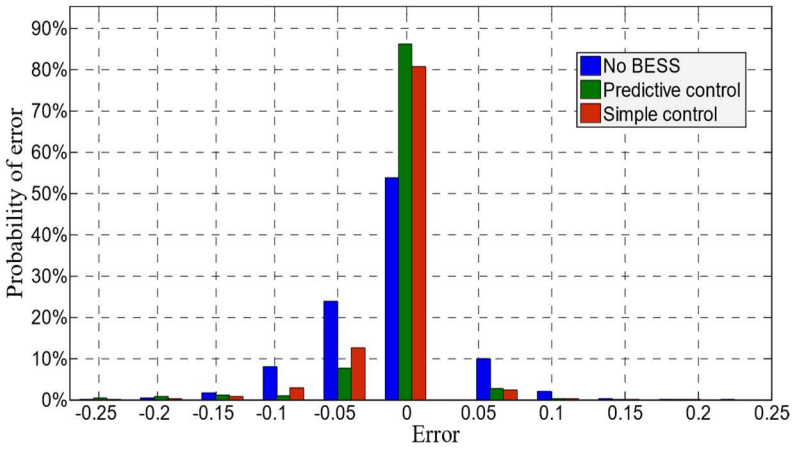

Figure 4-11 Histogram of error for the first scenario.

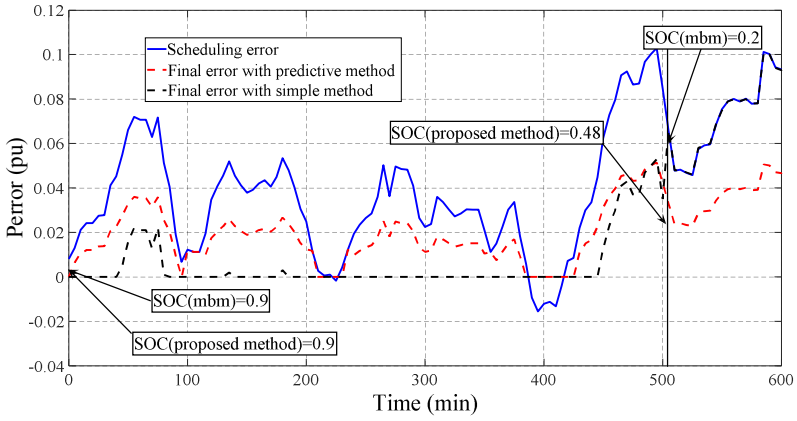

Figure 4-12 Performance comparison of different controllers during long underproduction period (positive scheduling error).

Table 4-1

Statistics of errors for the sample scenario

Method	Mean	Variance	MAE	RMSE
No BESS	-0.006	0.0023	0.0327	0.0482
Proposed	-0.002	0.0009	0.0179	0.0297
Simple	-0.002	0.0008	0.0178	0.0312

In Figure 4-12, positive P_{error} (solid blue line) indicates that the BESS should deliver energy to the grid. The simple controller (dotted black line) maintains the error at zero as much as possible by discharging the battery. Meanwhile, the predictive controller (dashed red line) maintains the error within ±5% and saves some energy for the end of this period when updated forecast data gives some estimates about future time steps. At t=500 min, the battery SOC with the simple controller reaches the minimum level; however, with the predictive controller, around 50% of the battery SOC still remains. Table 4-1 presents statistics of the forecast error for the aforementioned three cases. These statistics comprise

mean, variance, Mean Absolute Error (MAE), and Root Mean Square Error (RMSE). Utilizing the BESS with any controller decreases both MAE and RMSE.

Although errors associated with both simple and proposed controller have similar MAEs, RMSE of the proposed method is less than the simple controller. This implies that the proposed method is more successful in reducing the occasional large errors, where RMSE is more sensitive to large quantities. Figure 4-13 indicates the forecast error of the BPA wind system without using any energy storage. Figure 4-14 shows the forecast error of BPA system when BESS (P_{rated}=*0.15 pu,* E_{rated}=*0.55 pu)* is used.

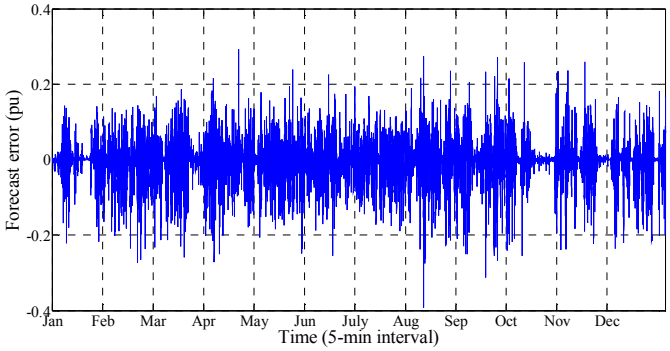

Figure 4-13 Forecast Error of BPA in 2013.

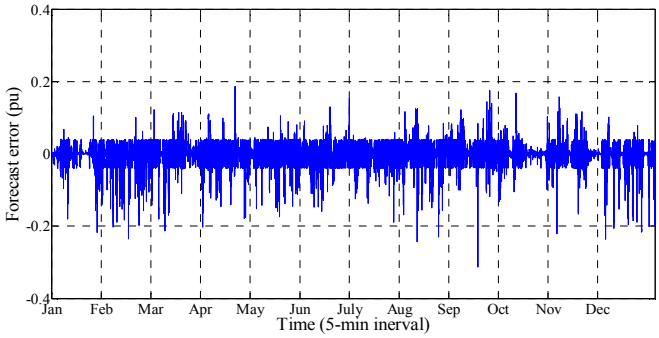

Figure 4-14 Forecast Error of BPA using BESS in 2013.

4.4.2 BESS Sizing

The probability of balanced energy with various power and energy ratings is depicted in Figure 4-15. It can be inferred that the energy capacity has more impact on battery availability than power rating. This statement is correct, since the amplitude of error is less than 0.15 pu 98.7% of the time. Therefore, increasing power rating affects the battery availability slightly. Keeping P^{B}_{rated} =0.15 pu as constant, Figure 4-16 demonstrates how the probability of balanced energy in a system with BESS depends not only on the energy rating of the battery, but also on the operation strategy. In order to meet the defined criteria in Section III, the BESS should be sized to have the balanced energy, at least, 90% of the time. In this case, the minimum required size of the battery with the simple controller is 0.44 pu. This energy rating is reduced to 0.37 pu for the battery by using the proposed method. A comparison between the proposed controller and 3 existing controllers (fuzzy, simple ANN, advanced ANN) in [10] is provided in Table 4-1. Note that, sizing comparison with the preceding research can be attained if the test case scenarios are similar. Allowable min and max limits of the SOC are set to 0 and 1 (SOC $\in$ [0,1]), in the mentioned reference. Thus, the same limits are for the SOC, and the simulations and sizing procedure are repeated. The cost function (4.9) is used to calculate the capital cost. It may be assumed that the BESS is connected to a 50-MW wind farm and all sizes and costs may be scaled to have a better sense for the real project. In this case, base values for power and energy are 50 MW and 50 MWh, respectively. It should be noted that this cost does not include base values for power and energy are 50 MW and 50 MWh, respectively. This cost does not include details like installation, commissioning, etc.

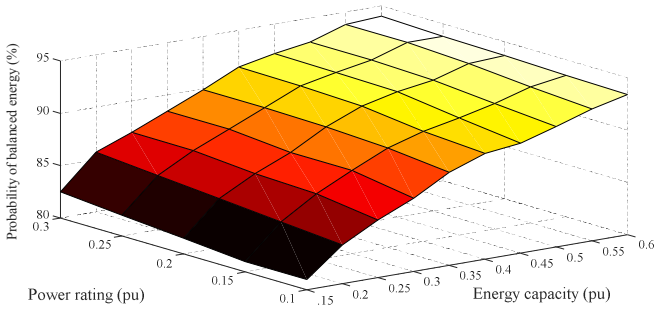

Figure 4-15 Probability of balanced energy for different power and energy ratings.

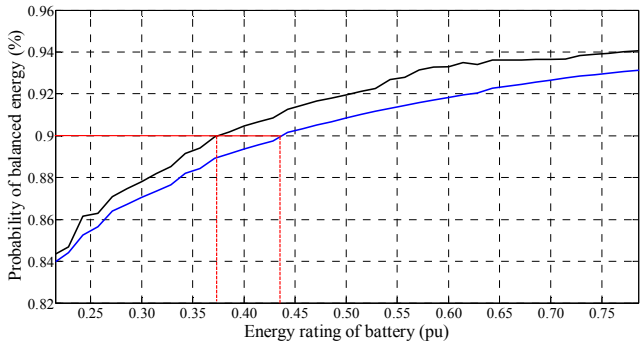

Figure 4-16 Probability of balanced energy with different energy capacity of BESS connected to a wind farm

Table 4-1

Sizing results with SOC between [0,1]

		proposed	simple	fuzzy	ANN	Adv. ANN
pu	P_{rated}	0.15	0.15	0.29	0.24	0.18
	E_{rated}	0.26	0.31	0.51	0.3	0.285
	cost	0.124	0.141	0.242	0.157	0.139
50-MW	P_{rated} (MW)	7.5	7.5	14.5	12	9
	E_{rated}(MWh)	13	15.5	25.5	15	14.5
	cost(M$)	6.2	7.05	12.1	7.8	6.97

Table 4-2

Lifetime estimation for simple and proposed methods

E_{rated}	0.2	0.25	0.3	0.35
Lifetime using proposed (yrs)	24.2	26.5	28.1	30.9
Lifetime using simple (yrs)	24.4	26.6	28.3	31.5

4.4.3 Battery Lifetime Analysis

The lifetime of the battery with the simple and proposed control strategy with different energy capacities is estimated by the algorithm presented in Figure 4-4 and results are given in Table 4-2. As expected, the battery lifetime analysis shows that the proposed method does not deteriorate battery depreciation. Typically, new methods of control can reduce battery lifetime when the number of charge/discharge cycles increases and deep discharging occurs more frequently. The expected lifetime of the battery with the control methods described in [10]- [11] is significantly reduced compared to the simple controller. However, the proposed method in this thesis tends to prevent unnecessary deep discharging and even has slightly better expected lifetime compared to the simple controller.

4.5 Conclusion

High penetration of wind energy increases reserve requirements to compensate voltage and power variations. Utilizing battery energy storage systems along with large wind farms provides higher reliability, and reduces back-up energy requirements. Furthermore, various controls and coordination of BESS result in different levels of power availability. This

chapter presented a novel control method for charging/discharging to increase the power availability of BESS. This method reduces the required size of the battery where the BESS is assigned to maintain the output power of the wind/BESS combination within a specific tolerance (i.e. ±0.05 pu of error for 90% of the time). The predictive control method reduced the capital cost of the required battery for wind applications. Various control methods may result in various trends of charging/ discharging, and they tend to increase or decrease battery lifetime. A new method for battery lifetime assessment is introduced in this chapter to evaluate the impact of the proposed control method on battery lifetime depreciation. Battery lifetime analysis is performed for both scenarios, and results show that the proposed control strategy does not degrade battery lifetime when compared to the simple controller. Therefore, the proposed control method of battery not only provides more availability to deliver/absorb additional power, but also helps prevent reduction in expected lifetime of battery due to overuse.

CHAPTER 5: Optimal Sizing and Operation of Battery Energy Storage Systems connected to Wind Farms Participating in Electricity Markets

5.1 Introduction

Due to intermittency nature of Renewable Energy Sources (RES), their integration into power systems has become quite challenging. The need for higher reserves in presence of the RES to smooth out the unpredictable power fluctuations is inevitable. Researchers generally agree that developing grid-tied energy storage systems is a practical solution to facilitate the massive integration of RES. Deployment of Battery Energy Storage (BESS) in power systems is experiencing a significant growth in recent years.

Energy storage systems, depending on the technology, can play different roles in power systems including frequency regulation, peak shaving, voltage control, transmission and distribution system equipment deferral, and energy arbitrage [66] and [67]. Much research has been conducted to demonstrate the suitable services for each type of energy storage [68]- [69], out of which the BESS has been found to be the most promising type with the capability to participate in multiple services. This stems from the fact that BESS produces a fast response and has a high energy density. Moreover, it has the potential to be expanded from home- to grid-scale.

Presently, among the different RES technologies, wind power has the largest share of generation, and can participate in day-ahead (DA) markets. Should wind farms be equipped with energy storage systems, they may fulfill their production commitment in the DA market and buy/sell energy from/in the real time (RT) energy markets. RT markets are designed to balance the deviations between DA 2commitments and the actual power

demands [70]. RT market participants should be paid or charged for generation that exceeds or falls behind the DA commitments [71], in which case those transactions are based on real-time Locational Marginal Prices (LMP).

The real-time price is significantly influenced by various factors. In fact, excess of generation can result in very low - even negative - prices. On the hand, lack of generation or a congestion in the system can lead the price to be extremely high.

Short-term wind and price forecasts can be employed to efficiently manage battery energy exchange with the grid for the sake of profit maximization. Since wind generation and RT prices are best with uncertainties, no operation strategy can guarantee the global optimal solution. However, in order to effectively tackle this problem, e. In contrast with deterministic optimization methods, the RHC uses prediction of future states of variables, constraints, and inputs over a moving time horizon to repetitively solve the problem. This method has been utilized in different fields, such as supply chain management, economics and finance, mechatronics, microgrid control, to mention a few [72], [73], and [74].

The wind power and electricity price data are comprehensively analyzed to obtain proper forecast models. In some papers (e.g. [75]), Monte Carlo simulations have been performed using probabilistic models to generate wind data. Although there are reliable probabilistic wind models, there is a lack of appropriate models to address RT electricity prices. Actual historical data (DA and RT) for wind and electricity price for MISO is used in this work. An ARIMA model is developed for wind power forecast and a Ridge-regression for RT price forecast. In order to train, evaluate, and test the price forecast model, a 1-year historical data is utilized to increase the accuracy of the model.

The following nomenclature is used:

Indices and parameters

$t, \tau \in T$ Index of time step.

H Number of samples in prediction horizon.

C_{total}^{b} BESS capital investment [$].

C_{P}^{b}, C_{E}^{b} Inverter and battery costs [$/W, $/Wh].

$\overline{E}^{b}, \underline{E}^{b}$ maximum and minimum allowed battery energy level [MWh].

E_{rated}^{b} Rated BESS energy level [MWh].

$\overline{P}^{b}$ Rated BESS power [MW].

S_{P}^{V} Sensitivity of voltage respect to active power.

S_{Q}^{V} Sensitivity of voltage respect to reactive power.

$\beta, \eta^{c}, \eta^{d}$ Battery self-discharge, charge, and discharge efficiencies.

Δt Time resolution [hour].

Variables

E_{t}^{b} BESS energy level at time t [MWh].

P_{t}^{b} BESS power at time t [MW].

P_{t}^{cur} Curtailed wind power at time t [MW].

P_{t}^{pur} Amount of power should be purchased from day-ahead market at time t [MW].

P_{t}^{sch} Committed energy production at time t [MW].

P_t^W Wind generation at time t [MW].

Q_t^b BESS reactive power at time t [MVAR].

u_t^c, u_t^d Auxiliary binary variables for charging and discharging at time t.

π_t^{DA}, π_t^{RT} Day-ahead and real-time prices in energy market at time t [$/MWh].

Operator

f Generic operand.

$\hat{f}_{\tau|t}$ Estimate of f for time τ, issued at time t.

5.2 System Description

A general optimization problem is formulated, and all constraints are discussed in detail. Then, the BESS lifetime estimation is presented as a model for the battery degradation.

5.2.1 Formulation

The objective function is to maximize the profit of the operation of the BESS connected to the wind farm. The objective function should contain two elements to represent DA and RT terms. The objective function and the relevant constraints are presented as follows.

$$\underset{P^b, P^{cur}, P^{pur}}{\text{Max}} \sum_t \left((P_t^w - P_t^{cur} + P_t^b) \cdot \pi_t^{DA} - P_t^{pur} \cdot \pi_t^{RT} \right) \tag{5.1}$$

subject to
$\forall t$

$$\left| P_t^{sch} - \left(P_t^w - P_t^{cur} + P_t^b + P_t^{pur} \right) \right| \leq \alpha \cdot P_t^{sch} \tag{5.2}$$

$$P_t^{pur} \geq 0 \tag{5.3}$$

$$0 \leq P_t^{cur} \leq P_t^w \tag{5.4}$$

$$P_t^b \geq -u_t^c \cdot \overline{P}^b \tag{5.5}$$

$$P_t^b \leq u_t^d \cdot \overline{P}^b \tag{5.6}$$

$$u_t^c + u_t^d \leq 1 \tag{5.7}$$

$$E_{(t+1)}^b = \beta E_t^b - u_t^c P_t^b \Delta t \eta^c - u_t^d P_t^b \Delta t / \eta^d \tag{5.8}$$

$$\underline{E}^b \leq E_t^b \leq \overline{E}^b \tag{5.9}$$

In the formulation, constraint (5.2) guarantees that the DA schedule is met. The combined wind and BESS may buy energy from the RT market when needed. This means the BESS is not discharged when the RT price is relatively cheap. The BESS can be also charged through the excess of the wind generation or through purchasing power from the grid during low-priced times. Also, α is the allowable power deviation from the scheduled power. When α is equal to 0, no deviation from the DA schedule is allowed. In this thesis ±5% of error is considered acceptable, and therefore, α= 0.05 is selected. Constraints (5.3) - (5.6) represent the limits on purchased power, curtailed power, and the BESS output. The BESS cannot charge and discharge at the same time and this is represented by (5.7). Energy level update of the BESS and its limits are represented in (5.8) and (5.9), respectively. Please note that u_t^c and u_t^d is used in (5.8) to apply charge or discharge efficiency.

5.2.2 Voltage Constraint

The voltage sensitivity analysis in a power system can be calculated based on the well-known Jacobian Matrix. The matrix connects the magnitude and phase of the nodal voltages to the nodal active and reactive power injections. It can be formulated as follows:

$$\begin{bmatrix} dP \\ dQ \end{bmatrix} = \begin{bmatrix} J_1 & J_2 \\ J_3 & J_4 \end{bmatrix} \begin{bmatrix} d\theta \\ dV \end{bmatrix} \tag{5.10}$$

$$\begin{aligned} J_1 &= \frac{\partial P}{\partial \theta} \quad J_2 = \frac{\partial P}{\partial V} \\ J_3 &= \frac{\partial Q}{\partial \theta} \quad J_4 = \frac{\partial P}{\partial V} \end{aligned} \tag{5.11}$$

Where *dP* and *dQ* are vectors representing changes of injected active and reactive power in various buses. Also, $d\theta$ and *dV* are, respectively, phase and magnitude changes of bus voltages. To find the voltage magnitude sensitivity with respect to injected active power, *dQ* should be maintained zero.

$$\Delta Q = 0 \Rightarrow S_P^V = \frac{dV}{dP} = \left(J_2 - J_1 J_3^{-1} J_4\right)^{-1} \tag{5.12}$$

Table 5-1

Results of the sensitivity analysis

s_P^V	s_Q^V	P_{base}^b	$\hat{P}_t^{inj}\ limit(\Delta Q = 0)$
0.12	12.6	250 MW	20.8 MW

Where *dP* and *dV* are in per units and S_P^V is unitless. In a similar way, voltage sensitivity with respect to injected reactive power is:

$$\Delta P = 0 \Rightarrow S_Q^V = \frac{dV}{dQ} = \left(J_4 - J_3 J_1^{-1} J_2\right)^{-1} \tag{5.13}$$

By applying the superposition principle at the point of common coupling, the total voltage change, because of the changes in the active and reactive power, can be found from the following equation:

$$\Delta V = \Delta P \cdot S_P^V + \Delta Q \cdot S_Q^V \tag{5.14}$$

It is worth noting that this sensitivity analysis does not include the transformer tap-changer positions. Although this is a standard sensitivity analysis in transmission networks, it is not practical to apply on distribution networks, where there are numerous nodes and the size of the Jacobian matrix is extremely large.

The IEEE 118-bus standard system is selected as the test case and it is assumed that the wind farm is connected to bus 110. MATPOWER [76] is utilized in MATLAB to find Jacobian matrices and calculate sensitivities of the voltage at bus 110 with respect to the injected active and reactive powers at the same bus, $S_{P^{110}}^{V^{110}}$ and $S_{Q^{110}}^{V^{110}}$. Table 5-1 provides these sensitivities and required information to utilize equation (5.14). The intent is to keep voltage variations within 1% per unit *($|V_t - V_{t-1}| \leq 0.01$).* The following set of equations can be added to the aforementioned optimization problem in order to account the voltage constraint.

$$\underset{P^b, P^{cur}, P^{pur}}{\text{Max}} \sum_t \left((P_t^w - P_t^{cur} + P_t^b) \cdot \pi_t^{DA} - P_t^{pur} \cdot \pi_t^{RT} \right) \tag{5.15}$$

subject to Eqs. (2), (3), (4), (5), (6), (7), (8), (9), and

$$\left| \left(P_t^{inj} - P_{t-1}^{inj} \right) \cdot S_P^V + \left(Q_t^b - Q_{t-1}^b \right) \cdot S_Q^V \right| \leq 0.01 \tag{5.16}$$

$$P_t^{b^2} + Q_t^{b^2} \leq \overline{S}^{b^2} \tag{5.17}$$

$$P_t^{inj} = P_t^w - P_t^{cur} + P_t^b \tag{5.18}$$

Where P_t^{inj} is the injected power at the point of common coupling (PCC) and $\overline{S}^b$ is the BESS rated apparent power.

A. Battery Cost and Degradation Model

The battery degradation of Lithium-ion batteries is highly dependent on the Depth of Discharge (DoD) of each cycle. An accurate lifetime analysis and battery degradation modeling are not the focus of this thesis. Hence, a linear approximation of the per cycle battery degradation is used to account in the optimization model. The SOC of the battery is limited to avoid any deep discharge or overcharging during the operation. The objective function which includes the degradation term is presented as follows.

$$\underset{P^b, P^{cur}, P^{pur}}{\text{Max}} \sum_t \left((P_t^w - P_t^{cur} + P_t^b) \cdot \pi_t^{DA} - P_t^{pur} \cdot \pi_t^{RT} - P_t^b \cdot \frac{C_{total}^b \cdot \Delta t}{n^{cycle} \cdot \overline{E}^b} \right) \tag{5.19}$$

Where the time resolution (Δt) is 1/12 of an hour and n^{cycle} is 5000 and defined as the number of complete charge/discharge cycles that the battery can experience before its capacity falls below the minimum expected level. In this thesis, an assumption is made that the battery degradation is not correlated with the Depth of Discharge (DoD), defined as the percentage of the battery that has been discharged during a cycle. Also, C^b is calculated as below.

$$C_{total}^b = C_P^b \cdot \overline{P}^b + C_E^b \cdot E_{rated}^b \tag{5.20}$$

Where C_P^b and C_E^b are selected 0.22 ($/W) and 0.35 ($/Wh), respectively. It should be noted that this cost model does not include miscellaneous costs, such as installation and maintenance.

5.3 METHODOLOGY

In this section, a methodology based on a RHC is proposed for BESS operation to maximize its profit. In the first section, the basics of the RHC is reviewed and the proposed formulations is introduced. In the next section, new constraints are sought to represent voltage control at the point of common coupling (PCC). Finally, forecast methods for wind power and RT price are discussed in the last section.

5.3.1 Receding Horizon Control (RHC)

RHC or model predictive control can be considered as a type of feedback control [77]-[78]. The RHC shows a good performance for stochastic and nonlinear problems. However, the RHC is an inappropriate control method for real-time applications, where it increases the size of an optimization problem, and requires data estimations. Therefore, the RHC can be considered as a viable options to control systems with sample times, at least, in seconds.

The basic concept of the RHC is depicted in Figure 5-1. The optimization problem, at each time step, is solved over a fixed time horizon. Then, the first decision variables from this horizon is used. The prediction horizon, consequently, moves forward and the same procedure is repeated. It is worth noting that all previous wind and price information is available for the optimization problem at each iteration. Then, wind power and RT price data is forecasted over the prediction horizon.

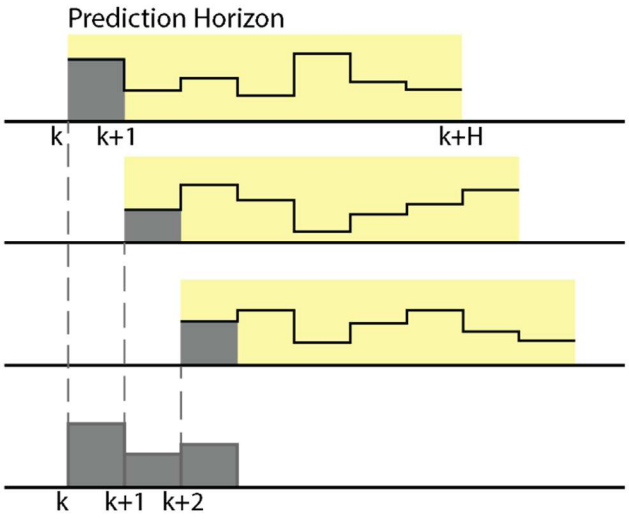

Figure 5-1 Schematic of Receding Horizon Control (RHC)

The optimization problem is solved based on the forecasted data, DA price, and committed wind production to maximize the profit. All constraints should be satisfied at each iteration to guarantee the feasibility of the solution. The objective is to maximize the profit in the current horizon with the following constraints:

$$\underset{P^b,P^{cur},P^{pur}}{\text{Max}} \sum_{t=1}^{T}\sum_{\tau=t+1}^{t+H}\left((\hat{P}^{w}_{\tau|t}-\hat{P}^{cur}_{\tau|t}+\hat{P}^{b}_{\tau|t})\cdot\pi^{DA}_{\tau}-\hat{P}^{pur}_{\tau|t}\cdot\hat{\pi}^{RT}_{\tau|t}\right) \tag{5.21}$$

$$\text{subject to} \quad \forall\,\tau\in[t+1,\ldots,t+H]$$

$$\left|P^{sch}_{\tau}-\left(\hat{P}^{w}_{\tau|t}-\hat{P}^{cur}_{\tau|t}+\hat{P}^{b}_{\tau|t}+\hat{P}^{pur}_{\tau|t}\right)\right|\le\alpha\cdot P^{sch}_{\tau} \tag{5.22}$$

$$\hat{P}^{pur}_{\tau|t}\ge 0 \tag{5.23}$$

$$0\le\hat{P}^{cur}_{\tau|t}\le\hat{P}^{w}_{\tau|t} \tag{5.24}$$

$$\hat{P}^b_{\tau|t} \le \hat{u}^d_{\tau|t} \cdot \overline{P}^b \tag{5.25}$$

$$\hat{P}^b_{\tau|t} \le -\hat{u}^c_{\tau|t} \cdot \overline{P}^b \tag{5.26}$$

$$\hat{u}^c_{\tau|t} + \hat{u}^d_{\tau|t} \le 1 \tag{5.27}$$

$$\hat{E}^b_{(\tau+1)|t} = \beta \cdot \hat{E}^b_{\tau|t} - \hat{u}^c_{\tau|t} \cdot \hat{P}^b_{\tau|t} \cdot \Delta t \cdot \eta^c - \hat{u}^d_{\tau|t} \cdot \hat{P}^b_{\tau|t} \cdot \Delta t / \eta^d \tag{5.28}$$

$$\underline{E}^b \le \hat{E}^b_{\tau|t} \le \overline{E}^b \tag{5.29}$$

$$\hat{E}^b_{t+1|t} = E^b_{t+1} \tag{5.30}$$

Constraint (30) guarantees the continuity of the state of charge of the battery while the optimization horizon moves forward. It is worth noting that E^b_{t+1} is obtained from (5.8). The flow chart of the proposed algorithm is presented in Figure 5-2. In order to limit the voltage variations at the PCC, the following set of equations should be solved.

$$\underset{P^b, P^{cur}, P^{pur}}{\text{Max}} \sum_{t=1}^{T} \sum_{\tau=t+1}^{t+H} \left((\hat{P}^w_{\tau|t} - \hat{P}^{cur}_{\tau|t} + \hat{P}^b_{\tau|t}) \cdot \pi^{DA}_{\tau} - \hat{P}^{pur}_{\tau|t} \cdot \hat{\pi}^{RT}_{\tau|t} \right) \tag{5.31}$$

subject to Eqs. (5.22)-(5.30) and

$$\left| \left(\hat{P}^{inj}_{\tau|t} - \hat{P}^{inj}_{\tau-1|t} \right) \cdot S^V_P + \left(\hat{Q}^b_{\tau|t} - \hat{Q}^b_{\tau-1|t} \right) \cdot S^V_Q \right| \le 0.01 \tag{5.32}$$

$$P^{b^2}_{\tau|t} + Q^{b^2}_{\tau|t} \le \overline{S}^{b^2} \tag{5.33}$$

Where the total injected power at point of common coupling can be found from the following:

$$\hat{P}^{inj}_{t} = \hat{P}^w_{\tau|t} - \hat{P}^{cur}_{\tau|t} + \hat{P}^b_{\tau|t} \tag{5.34}$$

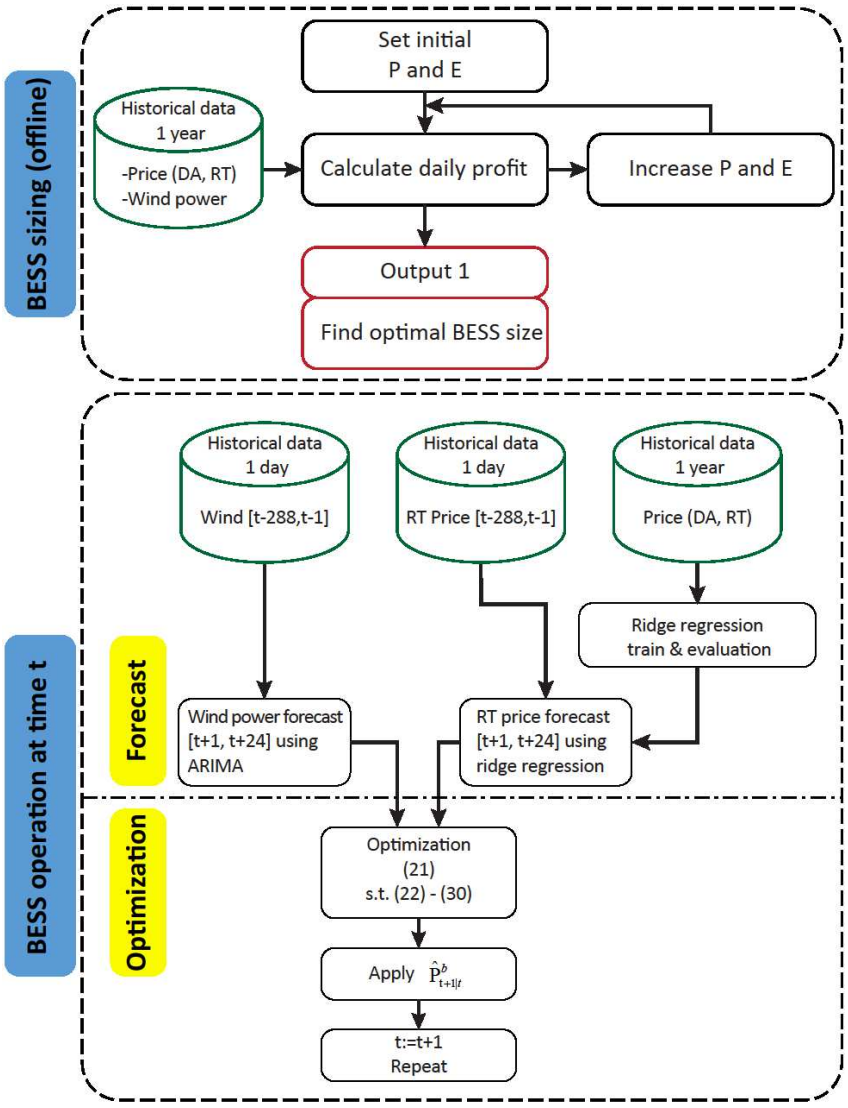

Figure 5-2 Flowchart of the proposed algorithm for BESS sizing and operation

5.3.2 Short-term Wind and Price Forecasts

Accurate wind power and electricity price forecasting can significantly influence the efficient operation of the BESS. Although the wind and price forecasting is not the main contribution of this thesis, workable approaches are developed to perform the forecasting tasks.

Wind and electricity are essential elements of short-term operations, as well as long-term planning. As a matter of fact, the efficient operation of a BESS depends on accurate short-term wind and price forecasts. Sampling resolution for wind in MISO is one hour and the prediction horizon is assumed to be 2 hours. Therefore, it is required to forecast two more data points. Traditional linear point forecast methods, such as auto regression-based models, does not provide the BESS models representing the non-stationarity of the wind [79]. Alternatively, probabilistic forecast methods account the uncertainties by quantifying them [80], [81], and [82].

Nevertheless, Auto Regression Integrated Moving Average (ARIMA) is used in this work where it is needed to forecast two data points and this is considered as a very short-term forecast. ARIMA models shows a good performance for a short-term wind forecast [83].

On the other hand, sampling resolution for RT price in MISO is 5 minutes. The prediction horizon is 2 hours and 24 data points should be forecasted in each step. According to [84], short-term price forecast includes forecasts from a minute up to a few days ahead. Most of the research in the literature focus on DA market and not RT market. Price forecast in RT market is basically Local Marginal Price (LMP) forecast which highly dependent on the network operations model and the congestion patterns [85]- [86] . In [86], LMP and network congestion forecast is considered from a system operator's perspective where there is an access to the power system operating conditions. In contrast, in this thesis, the problem is tackled from market participant's perspective is who does not have access to the private data and utilizes only publicly available historical data, such as LMP, zonal loads, wind, generation, DA market price, etc. A Ridge regression model is developed to forecast the RT price. Performance of a forecast method can be assessed through different

measures which are widely used in the literature such as Mean Absolute Error (MAE), Root Mean Square Error (RMSE), Mean Squared Error (MSE), or Mean Absolute Percentage Error (MAPE). The first two aforementioned indices are used to evaluate the performance of the forecast over a horizon at each step. The following equations represent MAE and RMSE, respectively, for wind power forecast at time step t:

$$MAE_t = \frac{1}{H}\sum_{\tau=1}^{H}\left|\hat{P}^w_{\tau|t} - P^w_{\tau}\right| \tag{5.35}$$

$$RMSE_t = \sqrt{\frac{1}{H}\sum_{\tau=1}^{H}\left(\hat{P}^w_{\tau|t} - P^w_{\tau}\right)^2} \tag{5.36}$$

Where H denotes the samples in each horizon. In this thesis, H would be 2 for wind forecast and 24 for RT price forecast. In order to generalize the indices for the total simulation time, they can be redefined as follows:

$$MAE_{Average} = \frac{1}{T \cdot H}\sum_{t=1}^{T}\sum_{\tau=1}^{H}\left|\hat{P}^w_{\tau|t} - P^w_{\tau}\right| \tag{5.37}$$

$$RMSE_{Total} = \frac{1}{T}\sum_{t=1}^{T}\sqrt{\frac{1}{H}\sum_{\tau=1}^{H}\left(\hat{P}^w_{\tau|t} - P^w_{\tau}\right)^2} \tag{5.38}$$

Where T denotes the total time intervals RHC is being performed in the simulation.

In this chapter, a time series model for wind power forecasting is developed. However, a detailed forecast approach for RT electricity price is provided in Appendix.

Wind Power Forecasting: Time series models (ARIMA, ARMA, ARX, etc) utilize the patterns of the previous points and movements over the time to forecast its future movements. General model of ARIMA is typically denoted by ARIMA (p,d,q) where p is

the order of lags in autoregressive model, d is the degree of differencing, and q is the order of lags in moving average model. In ARIMA, unlike ARMA, one can take the periodic difference between two data points and use them instead of the original data points to eliminate non-stationarity. It is worth mentioning that performance of time series forecast methods are acceptable once a series is stationary. The process of taking differences between two data points can be repeated until a stationary model is achieved.

The resolution of wind power data for MISO market is 1-hour and our prediction horizon is 2 hours. Although wind power data is non-stationary, its first degree of differencing becomes stationary. A general model of ARIMA (p,d,q) and the procedures of selecting its parameters are presented in [87]. In this thesis, ARIMA (3,1,3) is selected as the forecast model.

5.4 RESULTS

In this case study, wind power, DA and RT electricity price data for MISO are used. It is assumed that wind power is scheduled in the DA market and 5% deviation from scheduled power is acceptable at any time. If the actual wind power exceeds the scheduled power, and it deviates from the 5% tolerance, the excess energy should be either stored in the BESS or curtailed. Similarly, when the actual wind power is less than the scheduled power, the difference should be compensated by the BESS or the RT market. In this section, first the optimal size of an individual BESS connected to a 250-MW wind farm is found. Then, the operation of the BESS using RHC is assessed. The profitability of the BESS is compared to the no-BESS scenario and the best-case scenario with the perfect forecast. In the next part, the voltage constraint is taken into consideration and reassess the

performance of the BESS. In the last part of this section, the impact of the BESS price on its profitability is studied.

5.4.1 BESS Sizing

The historical wind power, DA and RT price data over a year is used, in this thesis, to find the optimal BESS size (power and energy ratings) with the aim of maximizing the profit. relatively long-term data (1 year) is used in order to avoid any biases in price or wind power due to seasonality issues. Figure 5-3 depicts the average daily profit of the BESS operation with different power and energy ratings. The BESS costs and degradation are considered in this process, where (5.19) is used as the objective function. Therefore, the higher size of the BESS does not necessarily increase the profit in long term. 40 MW and 120 MWh are selected, as power and energy ratings, respectively.

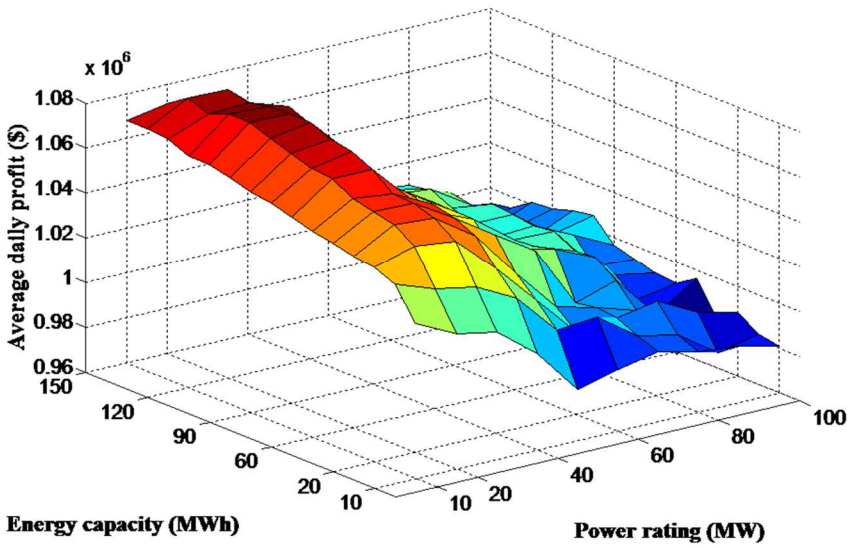

Figure 5-3 average daily profit for different energy and power ratings.

5.4.2 Average Daily Profit of BESS using RHC

In this thesis, the following items are assumed at any time step: 1) It is assumed that all publicly available historical data is accessible. 2) MCP cleared in DA market is available for the whole day. 3) There is no access to future actual wind power and RT price.

The optimization problem discussed in section III-A is implemented to calculate average daily profit from the operation of the BESS. At each iteration, the convex MILP problem is solved in Gurobi 7.5 [88], called by CVX [89] in MATLAB. Using a personal computer with a core i7 2.80-GHz CPU and8 GB of RAM, on average, it takes less than 2 seconds for each iteration.

Figure 5-4 shows the actual and scheduled wind power during the week. Also, the curtailed and purchased power are presented in Figure 5-5and the BESS operation results (output power and SOC) are presented in Figure 5-6. These figures demonstrate that the BESS absorbs some power between 24 and 48 hours and becomes fully charged. Therefore, the BESS cannot help with charging between 48 and 64 hours, and all excess of wind power is curtailed.

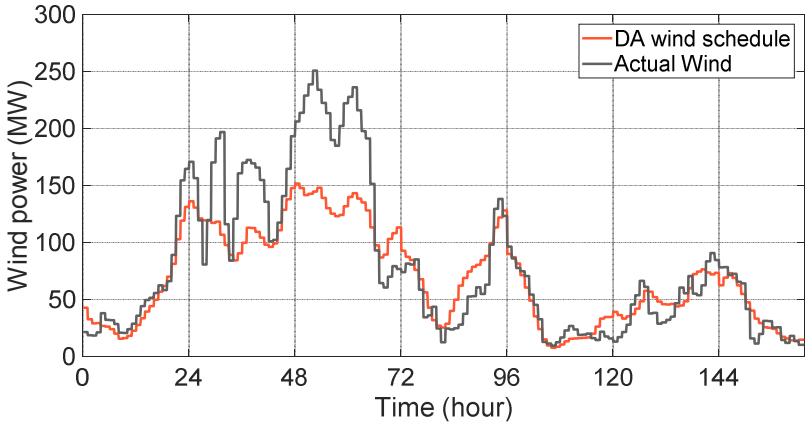

Figure 5-4 Actual and scheduled wind power.

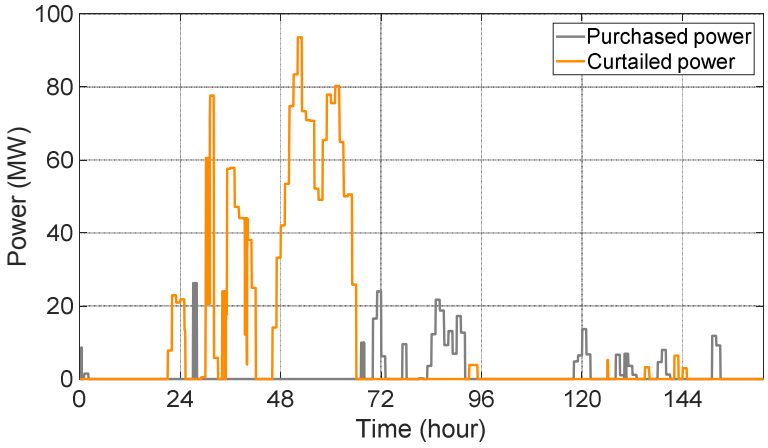

Figure 5-5 Purchased and curtailed power.

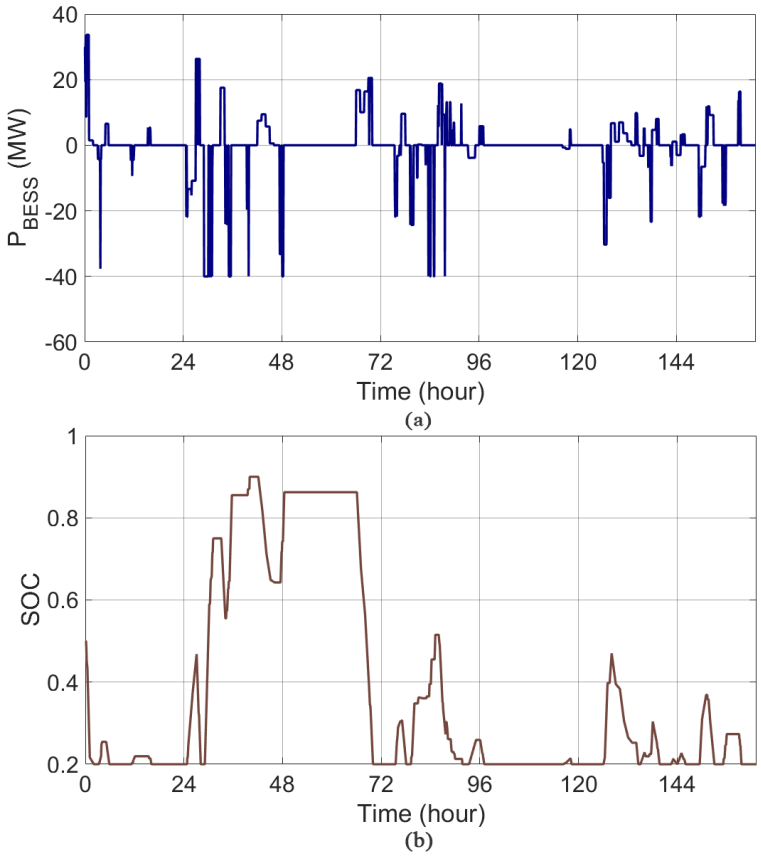

Figure 5-6 BESS active power output (a) and SOC (b) for a week.

5.4.3 Impact of Voltage Constraint

In this section, the performance and profitability of the BESS are evaluated in the presence of the voltage control constraints. For this reason, equations (5.26), (5.27) , and (5.28) shall be added to the previous optimization problem. It should be noted that this constraints keep the problem convex and tractable. The square function is convex for real values and it is supported in CVX. As mentioned, the IEEE 118-bus system is selected as the test case and use the results presented in Table 5-1. Also, Figure 5-7 demonstrates the BESS active and reactive power output when the voltage control is in effect. The results show that the reactive power is mostly limited to -4 and 4 MVAR and does not significantly affect the active power. Figure 5-7 illustrates the active and reactive power of the BESS with voltage control during the week. Results presented in Table 5-2 in section IV-C demonstrates that the average daily profit with voltage control is slightly less than the case without it.

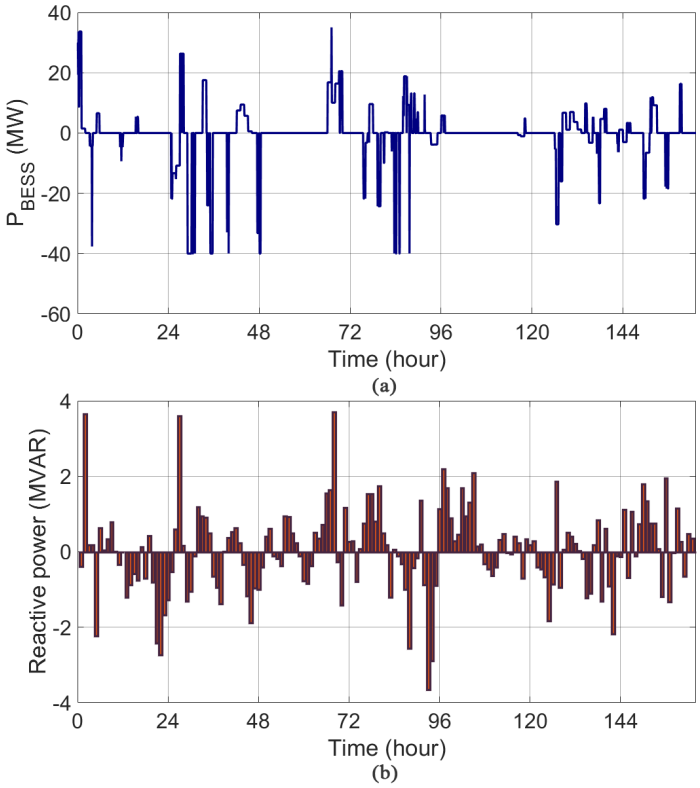

Figure 5-7 BESS active (a) and reactive (b) power output when voltage control is in effect.

5.4.4 Impact of the Battery Price and Degradation

The high cost of batteries is considered as the main obstacle for deployment of the BESS in power networks. However, battery costs have come down within the past decade, and is expected to be as low as 200 $/KWh for Li-ion in the next few years [90].

Impacts of the battery price and degradation on the profitability of the BESS are evaluated, in this section. Simulations with the objective function described in section II-C is performed and results are presented in Table 5-2. These results, as expected, show that the profit with the degradation model drops when the BESS operates less frequently. However, this results in lower battery degradation and higher lifetime expectancy. When the per cycle

value of the BESS operation is considered in the optimization problem, the higher profit in the long-term operation of the BESS can be expected.

Table 5-2

Average daily profit of various studies (p=40mwande=100mwh)

Scenario	Degradation	Voltage Control	Profit ($1000)		
			Total	Wind	BESS
1	-	-	608	573	35
2	-	✓	607	573	34
3	✓	-	601	573	28
4	✓	✓	600	573	27

5.5 CONCLUSION

The main challenge in power systems with high share of RES is to increase the flexibility of the system to maintain its balance. The BESS is an excellent candidate for mitigating adverse effects imposed by the RES. In this chapter, it is assumed that the BESS is co-located with the wind farm while participating in both DA and RT markets. When the wind power exceeds the DA scheduled power, the extra power must be curtailed or utilized to charge the BESS. On the contrary, if there is a lack of wind power, the difference between the actual and the scheduled power should be provided by the BESS or purchased from the

RT market. An optimization problem with the aim of maximizing the profit with all physical and operational constraints were formulated. First, the optimization problem was solved for 1-year historical wind power and electricity price data from MISO, to achieve the optimal size of the BESS. However, at the operation stage, it was assumed that the future wind power and RT electricity price values were not available. Therefore, the new RHC scheme using the forecasted data was proposed as an effective solution to deal with uncertainties. An ARIMA model for the wind power forecast and a ridge regression model for the RT electricity price forecast was developed and utilized in this chapter. Several scenarios were presented to assess the impact of the voltage control, the BESS lifetime, and the BESS price on the average daily profit.

CHAPTER 6: Conclusion and Future Work

In this thesis, the operation and sizing of single and hybrid energy storage systems in various scenarios were addressed. First, the interconnection requirements and the minimum power and energy requirement of energy storage systems in different cases were briefly addressed in this thesis. An analytical method for BESS sizing in presence of PV-induced ramp rate limits was proposed. In this method, locational impacts of the PV site have been considered, too. Moreover, a method for utilizing two or more energy storage technologies was introduced.

Control of the BESS has a great impact on its profitability. In this thesis, two scenarios were reviewed: 1- the wind farm does not participate in real-time market; 2- the wind farm participates in electricity market. In the first scenario, excess of wind power cannot be sold in the market and is counted as missed opportunity. In addition, the BESS is assumed to provide energy during times wind power is less than the DA scheduled power. However, in the second scenario, energy deficiency can be provided by the BESS or purchased from the RT market. Similarly, energy excess can be used to charge the batteries or sold into the RT market.

Each scenario is discussed in details and the physical and operational constraints were formulated. Each problem is solved through a Receding Horizon Control (RHC) or model predictive control scheme. A new method is proposed for the first scenario, which can be used in real-time applications.

The RHC based on updated wind and price forecast is proposed for the second scenario. The detailed conclusions and final remarks were provided in 6.1. The directions for future work on these topics were summarized in 6.2.

6.1 Concluding remarks and discussions

In chapter 3, different methods for sizing of energy storage systems has been discussed. It is worth noting that different utilities and regulators have different standards for integration of distributed generations. Different standards and requirements for high wind and PV integrations were reviewed. The minimum BESS size should be found based on the interconnection requirements in each system. In first part of Chapter 3, the requirements for the BESS to mitigate adverse effects of high PV penetration were reviewed.

Next, two methods to find the minimum power and energy required by grid were addressed. The analytic method is based on the worst-case scenario when PV generation drops (rises) 90%. Simulation of ramp rate control shows the trend of charging and discharging for a BESS connected to a PV plant. NREL historical data for simulation purposes is used.

Then, hybrid configuration of energy storage systems was proposed to mitigate wind energy fluctuations. Capital cost of energy storage systems is the main obstacle for them to be deployed. Much research has been conducted to increase efficiency and decrease the required size of ESS. Some types of ESS (like batteries) can respond rapidly and were suited to mitigate high frequency components of imbalance power. However, some other types of ESS are more efficient for slow cycles. DFT based method was used to break out slow and fast components of imbalance power. By using high and low pass filters, frequency domain

signal of imbalance power is decomposed and is transformed to the time domain by inverse DFT. In this chapter, a DFT-based coordinated strategy is introduced to distribute power between BESS and PSH. A methodology to determine power and energy capacity of each type of ESS was discussed. To validate the effectiveness of the proposed method, actual data of BPA for 2014 were used in the simulations.

Researchers may extend this work and use Discrete Fourier Transform (DFT) for operation of hybrid energy storage systems. One can forecast the few hours ahead using the past 24 hours' data. Then, the next few hours window can be divided into high frequency and low frequency components. One can assign low frequency components to PSH and then the amount combined PSH and wind output fall short of day-ahead schedule can be compensated by BESS.

In chapter 5, the opportunities for the BESS to participate in electricity market were reviewed. A BESS is a reliable resource to provide energy for various power system applications. The BESS can increase the flexibility and reliability of the renewable energy dispatch. Wind energy has the largest contribution among renewable energy resources and its control has become a research focus in power systems area.

In fact, the main challenge for battery to participate in a market is the high cost. Lifetime of batteries should be estimated and modeled as constraint in the optimization model.

In this chapter, it is assumed that the combined output power of the BESS and wind turbines should match with a DA scheduled power. If the wind power exceeds the scheduled power at any time interval, the extra wind power can be simply curtailed or used to charge the BESS. Meanwhile, during a wind energy deficiency, the deviated

power can be provided by the BESS or purchased from the RT market. It is assumed that ±5% is the allowable tolerance for deviation from the scheduled power.

A novel BESS control to manage the net energy exchange between a wind farm and the grid in an electricity market is introduced in this chapter. A Receding Horizon Control (RHC) scheme is proposed for optimal operation of the BESS in the presence of operational constraints. The proposed method seeks a decision policy to manage operation of the BESS to increase daily profits. Utilizing short-term wind and price forecasts provide valuable information for the BESS controller to obtain the best times to charge batteries, discharge the stored energy, or purchase energy from the DA market. An optimization problem is formulated considering BESS costs and operational constraints. This optimization problem, at each time step, was solved using the RHC scheme. All wind and electricity price data and case studies in this thesis are based on MISO energy market data.

6.2 Future Work

Interesting research directions for future work are recommended in this section. In what follows, detailed recommendations were discussed:

1- In Chapter 3, the planning stage of utilizing two or more energy storage technologies were addressed. The main challenge in this chapter is the issue of operation for hybrid energy storage systems. A good research direction could be operational concerns of hybrid energy storage systems. The balanced power can be forecasted and decomposed by algorithms proposed in chapter 3. The slower components can be assigned to PSH (or any slow ESS). The remaining error can be compensated by the BESS. However, deep research and detailed simulations are required to verify the

performance of the method and clarify possible challenges of utilizing this hybrid energy storage scheme.

2- In chapter 4, second life batteries can be considered as a cheaper option. Used batteries from EVs can be recycled and operated in other applications. Some repair and justifications should be done to make sure the used batteries can work properly in other applications. The second life batteries can support inverters with good amount of DC power. However, their energy capacity may be diminished after the first few years of use in EVs.

3- Chapter 5 could be extended by adding battery lifetime degradation into the constraints. The semi-empirical model of degradation, which is introduced in [10], can be utilized together with other sets of constraints in optimization problem. It should be noted that the model is not linear, but can be linearized within different sections. This constraints might be written and solved by a Mixed Integer Linear Programming MILP) solver.

4- In chapter 5, it was assumed that the power flow results of IEEE 118-bus system is maintained constant at each iteration. In other words, the voltage of the interconnected bus varies by the power injected or withdrew by the Wind-BESS. A detailed simulation could be done by putting wind farms at different buses. Therefore, power flows could be performed at each iteration and the results could be used in the optimization constraints. In actual systems, the current voltage of each bus can be read from the meter and utilized in the system.

5- Impact of location and seasonality could be an interesting factor to evaluate the profitability of the BESS in an electricity market. Different locations in a market

have different trends of electricity prices. First, the DA electricity price in an area can be higher or lower, on average, than another area. The average price in central California is less than that in southern California. Moreover, RT price can increase or decrease in different seasons. For example, the average southern California RT electricity price in the winter is less than in the summer. This is because southern California power system is more congested in the summer due to very high air conditioning loads [41].

References

[1] "Renewable Energy Policy Network for the 21st Century. Renewables 2007 Global Status Report [Online]. Available: http://goo.gl/x1FQlJ".

[2] "European Renewable Energy Council. Renewable Energy Technology Roadmap, 20% by 2020 [Online]. Available: http://goo.gl/j16z8R".

[3] G. N. Koutroumpezis and A. S. Saffigianni, "Optimum allocation of the maximum possible distributed generation penetration in a distribution network," *Electr. Power Syst. Res.,* vol. 80, no. 12, pp. 1421-1427, Dec. 2010.

[4] M. Beaudin, H. Zareipour, A. Schellenberglabe and W. Rosehart, "Energy storage for mitigating the variability of renewable electricity sources: An updated review," *Energy for Sustainable Development,* vol. 14, pp. 302-314, 2010.

[5] F. Díaz-González, A. Sumper , O. Gomis-Bellmunt and R. Villafáfila-Robles, "A review of energy storage technologies for wind power applications," *Renewable and Sustainable Energy Reviews,* vol. 16, no. 4, pp. 2154-2171, 2012.

[6] A. Dehamna, A. Eller and T. and Embury, "Energy Storage Tracker 4Q13," Navigant Research, Boulder, CO, 2014.

[7] D. Gautam and V. Vital, "Impact of Increased Penetration of DFIG-Based Wind Turbine Generators on Transient and Small Signal Stability of Power Systems," *IEEE Transactions on Power Systems,* vol. 24, no. 3, pp. 1426-1434, Aug. 2009.

[8] Y. Liu, W. Du, L. Xiao, H. Wang and K. Cao, "A Method for Sizing Energy Storage System to Increase Wind Penetration as Limited by Grid Frequency Deviations," *IEEE Trans. Power,* pp. 1-9, 2015.

[9] S. Mohajeryami, A. R. Neelakantan, I. Moghaddam and Z. Salami, "Modeling of Deadband Function of Governor Model and its Effect on Frequency Response Characteristics," in *North American Power Symposium (NAPS)*, 2015.

[10] T. K. Brekken, A. Yokochi, A. von Jouanne, Z. Z. Yen, H. M. Hapke and D. A. Halamay, "Optimal energy storage sizing and control for wind power applications," *IEEE Transactions on Sustainable Energy,* vol. 2, no. 1, pp. 69-77, Jan. 2011.

[11] X. Ke, N. Lu and C. Jin, "Control and size energy storage systems for managing energy imbalance of variable generation resources," *IEEE Transactions on Sustainable Energy,* vol. 6, no. 1, pp. 70-78, Jan. 2015.

[12] S. Dutta and R. Sahrma, "Optimal storage sizing for integrating wind and load forecast uncertainties," in *IEEE PES Innovative Smart Grid Technologies (ISGT)*, 2012.

[13] C. Abbey and G. Joos, "A stochastic optimization approach to rating of energy storage systems in wind-diesel isolated grids," *IEEE Transactions on Power Systems,* vol. 24, no. 1, pp. 418- 426, Feb. 2009.

[14] A. Oudalov, D. Chartouni and C. Ohler, "Optimizing a battery energy storage system for primary frequency control," *IEEE Transactions on Power Systems,* vol. 22, no. 3, pp. 1259-1266, Aug. 2007.

[15] Y. M. Atwa and E. F. El-Saadany, "Optimal allocation of ESS in distribution systems with a high penetration of wind energy," *IEEE Transactions on Power Systems,* vol. 25, no. 4, pp. 1-8, Nov. 2010.

[16] P. Pinson, G. Papaefthymiou, B. Klockl and J. Verboomen, "Dynamic sizing of energy storage for hedging wind power forecast uncertainty," in *IEEE Power & Energy Society General Meeting*, 2009.

[17] F. Luo, K. Meng, Z. Y. Dong, Y. Zheng , Y. Chen and K. P. Wong, "Coordinated operational planning for wind farm with battery energy storage system," *IEEE Transactions on Sustainable Energy,* vol. 6, no. 1, pp. 253-262, 2015.

[18] Y. V. Makarov, P. Du, M. C. W. Kintner-Meyer, C. Jin and H. F. Illian, "Sizing energy storage to accommodate high penetration of variable energy resources," *IEEE Transactions on Sustainable Energy,* vol. 3, no. 1, pp. 34- 40, Jan. 2012.

[19] J. Xiao, L. Bai, F. Li, L. Haishen and C. Wang, "Sizing of Energy Storage and Diesel Generators in an Isolated Microgrid Using Discrete Fourier Transform (DFT)," *IEEE Transactions on Sustainable Energy,* vol. 5, no. 3, pp. 907- 916, July 2014.

[20] H. Bitaraf, S. Rahman and M. Pipattanasomporn, "Sizing Energy Storage to Mitigate Wind Power Forecast Error Impacts by Signal Processing Techniques," *IEEE Transactions on Sustainable Energy,* vol. 6, no. 4, pp. 1457-1465, Oct. 2015.

[21] Q. Jiang and H. Hong, "Wavelet-Based Capacity Configuration and Coordinated Control of Hybrid Energy Storage System for Smoothing Out Wind Power Fluctuations," *IEEE Transactions on Power Systems,* vol. 28, no. 2, pp. 1363- 1372, May 2013.

[22] C. Bueno and J. A. Carta, "Wind powered pumped hydro storage systems, a means of increasing the penetration of renewable energy in the Canary Islands," *Renewable and Sustainable Energy Reviews,* vol. 10, no. 4, pp. 312-340, Aug. 2006.

[23] F. Qiang and e. al, "Microgrid Generation Capacity Design With Renewables and Energy Storage Addressing Power Quality and Surety," *IEEE Transactions on Smart Grid,* vol. 3, no. 4, pp. 2019-2027, Dec. 2012.

[24] P. M. Carvalho, P. F. Correia and L. A. Ferreira, "Distributed reactive power generation control for voltage rise mitigation in distribution networks," *IEEE Transactions on Power Systems,* vol. 23, no. 2, pp. 766-772, May 2008.

[25] J. M. Gants, S. M. Amin and A. M. Giacomoni, "Optimal mix and placement of energy storage systems in power distribution networks for reduced outage costs," *IEEE Energy Conversion Congress and Exposition (ECCE),* pp. 2447-2453, 15-20 Sept. 2012.

[26] N. Lu, M. R. Weimar, Y. V. Makarov and C. Loutan, "An evaluation of the NaS battery storage potential for providing regulation service in California," in *Power Systems Conference and Exposition (PSCE), 2011 IEEE/PES*, 2011.

[27] T. Sels, C. Dragu, T. Van Craenenbroeck and R. Belmans, "Overview of new energy storage systems for an improved power quality and load managing on distribution level," *Proc. 16th Intl. Conf. and Exibition on Electricity Distribution, Part 1: Contributions,* pp. 1-5, 2001.

[28] A. Oudalov, R. Cherkaoui and A. Beguin, "Sizing and Optimal Operation of Battery Energy Storage System for Peak Shaving Application," *Proc. IEEE Lausanne Powertech,* pp. 621-625, Lausanne, Switzerland, 2007.

[29] J. P. Barton and D. Infield, "Energy storage and its use with intermittent renewable energy," *IEEE Transactions on Energy Conversion,* vol. 19, no. 2, pp. 441-448, Jun. 2004.

[30] D. Wu, C. Jin, P. Balducci and M. Kintner-Meyer, "An energy storage assessment: Using optimal control strategies to capture multiple services," *2015 IEEE Power & Energy Society General Meeting,* pp. 1-5, July 2015.

[31] S. Teleke, M. E. Baran, A. Q. Huang, S. Bhattacharya and L. Anderson, "Control Strategies for Battery Energy Storage for Wind Farm Dispatching," *IEEE Transactions on Energy Conversion,* vol. 24, no. 3, pp. 725-732, Jun. 2009.

[32] A. Damiano, G. Gatto, I. Marongiu, M. Porru and A. Serpi, "Real-time control strategy of energy storage systems for renewable energy sources exploitation," *IEEE Transactions on Sustainable Energy,* vol. 5, pp. 567-576, 2014.

[33] R. Walawalkar, J. Apt and R. Mancini, "Economics of electric energy storage for energy arbitrage and regulation in New York," *Energy Policy,* vol. 35, pp. 2558-2568, 2007.

[34] N. Lu, M. R. Weimar, Y. V. Makarov, J. Ma and V. V. Viswanathan, "The wide-area energy storage and management system—Battery storage evaluation," *PNNL-18679, Pacific Northwest National Laboratory, Richland, WA, USA,* 2009.

[35] S. X. Chen, H. B. Gooi and M. Wang, "Sizing of energy storage for microgrids," *IEEE Transactions on Smart Grid,* vol. 3, pp. 142-151, 2012.

[36] Q. Fu, L. F. Montoya, A. Solanki, A. Nasiri, V. Bhavaraju, T. Abdallah and C. Y. David, "Microgrid generation capacity design with renewables and energy storage addressing power quality and surety," *IEEE Transactions on Smart Grid,* vol. 3, pp. 2019-2027, 2012.

[37] Z. Hu, F. Zhang and B. Li, "Transmission expansion planning considering the deployment of energy storage systems," in *IEEE Power and Energy Society General Meeting*, San Diego, CA, USA, July 2012.

[38] M. Brenna, E. Tironi and G. Ubezio, "Proposal of a local dc distribution network with distributed energy resources," in *Proc. IEEE ICHQP*, Lake Placid, NY, USA, 2004.

[39] M. Dicorato, G. Forte, M. Pisani and M. Trovato, "Planning and operating combined wind-storage system in electricity market," *IEEE Transactions on Sustainable Energy,* vol. 3, pp. 209-217, 2012.

[40] Z. Wang, C. Gu, F. Li, P. Bale and H. Sun, "Active demand response using shared energy storage for household energy management," *IEEE Transactions on Smart Grid,* vol. 4, pp. 1888-1897, 2013.

[41] H. Mohsenian-Rad, "Optimal bidding, scheduling, and deployment of battery systems in California day-ahead energy market," *IEEE Transactions on Power Systems,* vol. 31, pp. 442-453, 2016.

[42] H. Mohsenian-Rad, "Coordinated price-maker operation of large energy storage units in nodal energy markets," *IEEE Transactions on Power Systems,* vol. 31, pp. 786-797, 2016.

[43] N. Lu, J. H. Chow and A. A. Desrochers, "Pumped-storage hydro-turbine bidding strategies in competitive electricity market," *IEEE Transactions on Power Systems,* vol. 19, no. 2, pp. 834-841, 2004.

[44] D. Perekhodtstev, "Two essays on problems of deregulated electricity market," PhD Dissertation (Carnegie Mellon University), 2004.

[45] R. Deb, "Operation hydroelectric plants and pumped storage units in a competitive environment," *The Electricity Journal,* pp. 24-32, 2000.

[46] J. Kazempour, M. Parsa Moghaddam, M. Haghifam and G. R. Yousefi, "Electric energy storage systems in a market-based economy: Comparison of emerging and traditional technologies," *Renewable Energy,* p. 2630–2639, 2009.

[47] A. Karimi Varkani, A. Daraeepour and H. Monsef, "A new self-scheduling strategy for integrated operation of wind and pumped-storage power plants in power markets," *Applied Energy,* p. 5002–5012, 2011.

[48] D. K. Khatod, V. Pant and J. Sharma, "Optimized daily scheduling of wind-pumped hydro plants for a day-ahead electricity market system," in *International Conference on Power Systems*, 2009.

[49] F. B. J. J. a. G. K. L. Costa, "Management of energy storage coordinated with wind power under electricity market conditions," in *Proc. Probabilistic Methods Appl. Power Syst. (PMAPS)*, 2008.

[50] G. F. M. P. a. M. T. M. Dicorato, "Planning and operating combined wind-storage system in electricity market," *IEEE Trans. Sustain. Energy,* vol. 3, pp. 209-217, Apr 2012.

[51] H. Akhavan-Hejazi and H. Mohsenian-Rad, "Optimal Operation of Independent Storage Systems in Energy and Reserve Markets With High Wind Penetration," *IEEE Transaction on Smart Grid,* vol. 5, pp. 1088-1097, 2014.

[52] A. Damiano, G. Gatto, I. Marongiu, M. Porru and A. Serpi, "Real-Time Control Strategy of Energy Storage Systems for Renewable Energy Sources Exploitation," *IEEE Transactions on Sustainable Energy,* vol. 5, no. 2, pp. 567-576, Apr. 2014.

[53] P. Kou, D. Liang, F. Gao and L. Gao, "Coordinated Predictive Control of DFIG-Based Wind-Battery Hybrid Systems: Using Non-Gaussian Wind Power Predictive Distributions," *IEEE Transactions on Energy Conversion,* vol. 30, pp. 681-695, 6 2015.

[54] P. Kou, F. Gao and X. Guan, "Stochastic predictive control of battery energy storage for wind farm dispatching: Using probabilistic wind power forecasts," *Renewable Energy,* vol. 80, pp. 286-300, 2015.

[55] H. Chitsaz, P. Zamani-Dehkordi, H. Zareipour and P. Parikh, "Electricity Price Forecasting for Operational Scheduling of Behind-the-meter Storage Systems," *IEEE Transactions on Smart Grid,* vol. PP, pp. 1-12, 2017.

[56] J. Marcos, I. de la Parra and M. García an, "Control Strategies to Smooth Short-Term Power Fluctuations in Large Photovoltaic Plants Using Battery Storage Systems," *Energies,* pp. 6593-6619, 2014.

[57] "Historical Data of Wind Generation and Wind Forecast in 2014, Bonneville Power Administration (BPA) Portland, OR, USA [online]. Available: http://transmission.bpa.gov/business/ operations/wind/," [Online].

[58] D. Bazargan, S. Filizadeh and A. M. Gole, "Stability Analysis of Converter-Connected Battery Energy Storage Systems in the Grid," *IEEE Transactions on Sustainable Energy,* vol. 5, no. 4, pp. 1204-1212, Oct. 2014.

[59] "ASTM E 1049-85. (Reapproved 2011), Standard Practices for Cycle Counting in Fatigue Analysis. American society for testing and materials (ASTM) International, West Conshohocken, PA, USA, 2011.".

[60] S. D. Downing and D. F. Socie, "Simple rain flow counting algorithms," *International Journal of Fatigue,* vol. 4, pp. 31-40, 1982.

[61] X. Ke, N. Lu and C. Jin, "Control and size energy storage systems for managing energy imbalance of variable generation resources," *IEEE Transactions on Sustainable Energy,* vol. 6, pp. 70-78, 2015.

[62] B. Foggo and N. Yu, "Improved Battery Storage Valuation Through Degradation Reduction," *IEEE Transactions on Smart Grid,* pp. 1-13, 2017.

[63] "Vice RL. Balancing resources and demand standards: BAL-007 through BAL-011; 2006. < http://www.nerc.com/docs/standards/sar/BAL-007-011_clean_last_posting_30-day_Pre-ballot_06Feb07.pdf >".

[64] N. Jaleeli and L. S. VanSlyck, "NERC's new control performance standards," *IEEE Transactions on Power Systems,* vol. 14, no. 3, pp. 1092-1099, Aug. 1999.

[65] "Bonneville Power Administration website [Online]. Available: https://www.bpa.gov".

[66] J. P. Barton and D. G. Infield, "Energy storage and its use with intermittent renewable energy," *IEEE Transactions on Energy Conversion,* vol. 19, pp. 441-448, 6 2004.

[67] K. C. Divya and J. {\O}stergaard, "Battery energy storage technology for power systems_An overview," *Electric Power Systems Research,* vol. 79, pp. 511-520, 2009.

[68] B. Dunn, H. Kamath and J.-M. Tarascon, "Electrical energy storage for the grid: a battery of choices," *Science,* vol. 334, pp. 928-935, 2011.

[69] "Overview of current development in electrical energy storage technologies and the application potential in power system operation," *Applied Energy,* vol. 137, pp. 511-536, 2015.

[70] J. M. Morales, A. J. Conejo, H. Madsen, P. Pinson and M. Zugno, Integrating renewables in electricity markets: operational problems, vol. 205, Springer Science & Business Media, 2013.

[71] *https://www.iso-ne.com/markets-operations/markets/da-rt-energy-markets ,* 2016.

[72] J. Mattingley, Y. Wang and S. Boyd, "Code generation for receding horizon control," in *Computer-Aided Control System Design (CACSD), 2010 IEEE International Symposium on*, 2010.

[73] M. Vukov, S. Gros, G. Horn, G. Frison, K. Geebelen, J. B. J{\o}rgensen, J. Swevers and M. Diehl, "Real-time nonlinear MPC and MHE for a large-scale mechatronic application," *Control Engineering Practice,* vol. 45, pp. 64-78, 2015.

[74] A. Parisio, E. Rikos and L. Glielmo, "A model predictive control approach to microgrid operation optimization," *IEEE Transactions on Control Systems Technology,* vol. 22, pp. 1813-1827, 2014.

[75] Y. Xu, Q. Hu and F. Li, "Probabilistic model of payment cost minimization considering wind power and its uncertainty," *IEEE Transactions on Sustainable Energy,* vol. 4, pp. 716-724, 2013.

[76] R. D. Zimmerman, C. E. Murillo-Sanchez and R. J. Thomas, "MATPOWER: Steady-State Operations, Planning, and Analysis Tools for Power Systems Research and Education," *IEEE Transactions on Power Systems,* vol. 26, pp. 12-19, 2 2011.

[77] W. H. Kwon and S. H. Han, Receding horizon control: model predictive control for state models, Springer Science & Business Media, 2006.

[78] G. Goodwin, M. M. Seron and J. A. De Don{\'a}, Constrained control and estimation: an optimisation approach, Springer Science & Business Media, 2006.

[79] C. Wan, Z. Xu, P. Pinson, Z. Y. Dong and K. P. Wong, "Probabilistic forecasting of wind power generation using extreme learning machine," *IEEE Transactions on Power Systems,* vol. 29, pp. 1033-1044, 2014.

[80] C. Wan, Z. Xu, Y. Wang, Z. Y. Dong and K. P. Wong, "A hybrid approach for probabilistic forecasting of electricity price," *IEEE Transactions on Smart Grid,* vol. 5, pp. 463-470, 2014.

[81] T. Hong, P. Pinson, S. Fan, H. Zareipour, A. Troccoli and R. J. Hyndman, *Probabilistic energy forecasting: Global energy forecasting competition 2014 and beyond,* Elsevier, 2016.

[82] C. Wan, M. Niu, Y. Song and Z. Xu, "Pareto optimal prediction intervals of electricity price," *IEEE Transactions on Power Systems,* vol. 32, pp. 817-819, 2017.

[83] R. G. Kavasseri and K. Seetharaman, "Day-ahead wind speed forecasting using f-ARIMA models," *Renewable Energy,* vol. 34, pp. 1388-1393, 2009.

[84] R. Weron, "Electricity price forecasting: A review of the state-of-the-art with a look into the future," *International journal of forecasting,* vol. 30, pp. 1030-1081, 2014.

[85] M. Sahni, R. Jones and Y. Cheng, "Beyond the crystal ball: locational marginal price forecasting and predictive operations in US power markets," *IEEE Power and Energy Magazine,* vol. 10, pp. 35-42, 2012.

[86] Y. Ji, R. J. Thomas and L. Tong, "Probabilistic forecasting of real-time LMP and network congestion," *IEEE Transactions on Power Systems,* vol. 32, pp. 831-841, 2017.

[87] N. Amjady, "Short-term hourly load forecasting using time-series modeling with peak load estimation capability," *IEEE Transactions on Power Systems,* vol. 16, pp. 798-805, 11 2001.

[88] I. Gurobi Optimization, "Gurobi Optimizer Reference Manual; 2015," *URL http://www. gurobi. com,* 2016.

[89] M. Grant, S. Boyd and Y. Ye, *CVX: Matlab software for disciplined convex programming,* 2008.

[90] R. Kempener and E. Borden, "Battery storage for renewables: market status and technology outlook," *International Renewable Energy Agency (IRENA): Abu Dhabi, UAE,* 2015.

Appendix

RT Electricity Price Forecasting: In order to carry out a thorough data analysis for RT electricity price forecast, our work is split into four main categories. In what follows, each category and its necessary components are provided.

1) Data gathering and pre-processing: all historical price (DA and RT), load, and weather data are gathered for anode in Riverside, Missouri. Then, missing values are imputed, and outliers are replaced with the previous bounded data.

2) Feature engineering: In this step, several features for analyzing the data are created such as DA price, load, temperature, renewable generation, and their seasonal features (hour, day, weekday/weekend, and month).

3) Historical DA and RT prices, historical load and demand forecast, imports/exports, historical reserve calls, renewable generations, calendar effects (day, hour, month) influence the electricity price . Some features like historical reserve calls are not publicly available. In this thesis, features are created based on the available data. In order to select the BESS features, the correlation between each feature and the actual RT price is evaluated in the first stage. Some features are highly correlated and carries a high level of dependency to the target variable (RT price). These relevant features include temperature forecast, historical DA and RT prices, historical load, and demand forecast. However, some features are not highly correlated with the RT price (e.g. calendar effects, renewable generation, generation types, etc.), which should be eliminated. In the next stage, redundant features should be detected and filtered, while working on the remaining relevant features from the

first stage. The correlation of every two features should be examined to evaluate whether a set of two features carry similar information about the target variable. For instance, temperature and load are highly correlated. This means one of them can be eliminated

4) Exploratory analysis: In this step, it is required to evaluate different characteristics of data sets. Exploratory analysis is typically applied before model developments to eliminate or sharpen hypotheses about the data. Univariate statistical analysis techniques applied in this thesis include outlier detection, central tendency and spread statistics (e.g. mean, median, distribution, interquartile range, etc.), and seasonality assessment. Moreover, multivariate statistical analysis techniques are applied to highlight the relationship between two or more variables. For instance, simple correlations are used to rank the importance of different features in feature selection stage. Figure A-1 demonstrates the correlation between RT price and some features, such as 5-minute lag, 120-minute lag, and load.

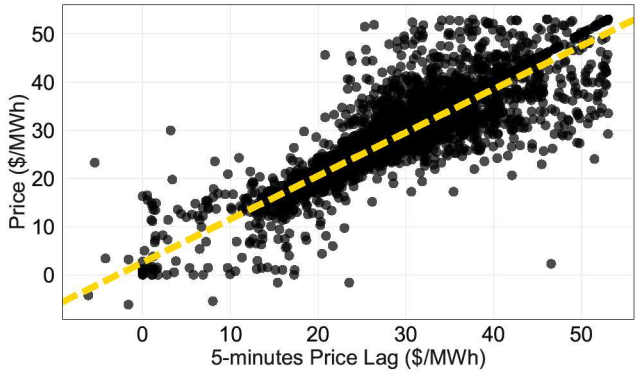

(a)

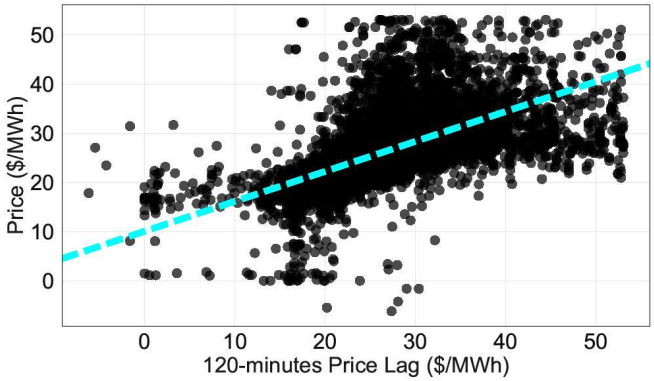

(b)

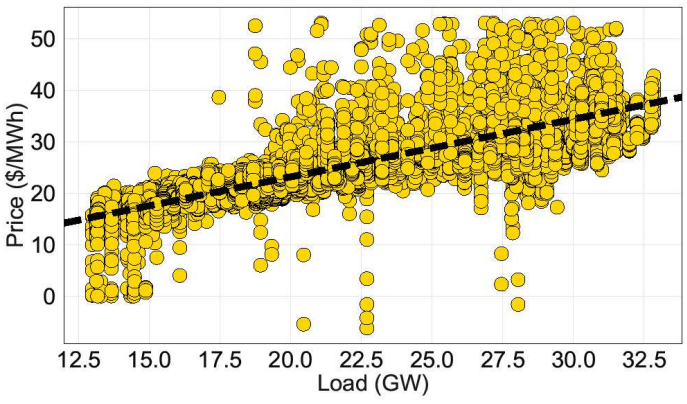

(c)

Figure A-1 Illustration of correlation between RT electricity price and last 5-minute (a), last 120-minute (b), and load (c) features.

5) Data-driven forecast model development: It is needed to perform the forecast process every 5 minutes. At each iteration, it is intended to forecast 24 values, which are RT prices for the next two hours with 5-minute resolutions. The forecast model maps input values from the selected features to outputs (RT prices). Much research has been conducted in the area of DA price forecast and numerous approaches have been introduced. A comprehensive review of various forecasting models for DA electricity price is provided in [4]. However, only a published studies consider the short-term RT price forecasting problem. Since, the RT price forecasting is not the main focus of this thesis, a simple ridge regression model is selected to implement in this work. The standard form of multiple linear regression can be written as follows.

Where $Y_{n\times1}$ represents target variables (RT price), $X_{n\times1}$ with the rank of m represents independent variables, $\beta_{m\times1}$ represents regression coefficients. Also, e is the vector of the residual errors with $E[e] = 0$ and $E[ee'] = \sigma_n^2$, where $E[.]$ is the expected value operator. It is worth noting that $\beta_{m\times1}$ is unknown and should be estimated through the historical training data (06/01/2016 to08/15/2016). The ridge regression estimates the coefficients by solving a problem in the following form:

Where $\alpha \geq 0$ is the regularization parameter, which imposes a penalty on the size of the coefficients and reduces the variance. The best regularization parameter (α) is selected by performing the Leave-One-Out cross-validation technique.

2-6) Performance evaluation: the data is divided into three sets to use in training, validation, and forecast periods. The historical data from June 1 until August 15, 2016, is used for training. Also, the historical data from August 15 until August 22, 2016, is used in the

validation stage. Finally, the forecast process is performed on the historical data from August 23 until August 29, 2016. It is worth mentioning that the forecast process is performed every 5 minutes for a two-hour prediction horizon. The price forecast results for 5, 60, and 120 minutes ahead are presented in Fig. A.1.

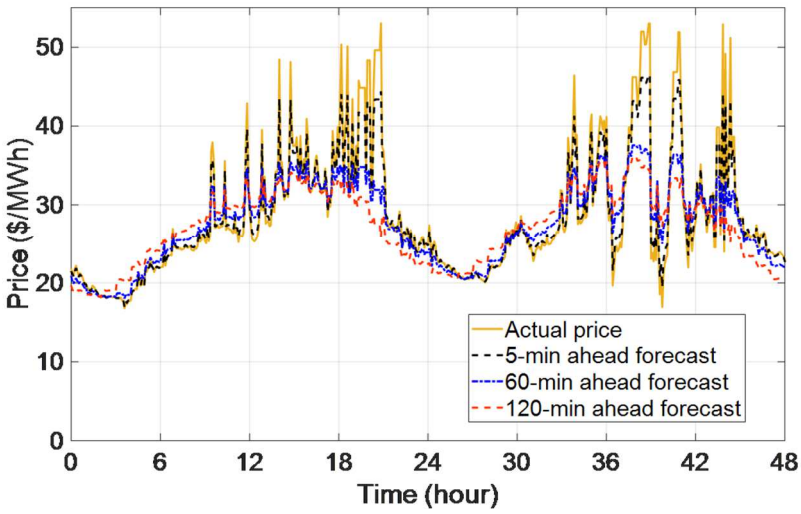

Figure A.2 Price forecast for three different lags (5, 60, and 120 minutes ahead).

In order to assess the performance of the adopted forecasting approach, the Root Mean Square Error (RMSE) as a well-established statistical metric is utilized and results are presented in Fig. A-3.

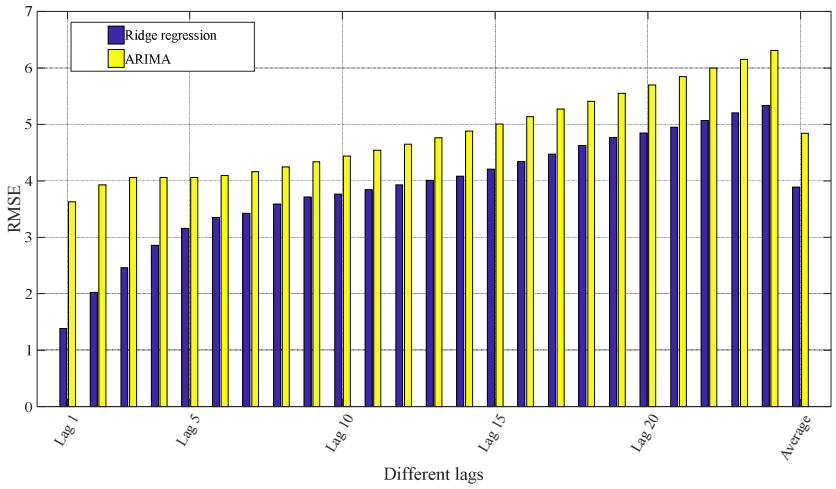

Figure A.3 RMSE of errors for various lags (lag 1 represents 5-minute ahead, lag 2 represents 10-minute ahead, and etc.).